DEVELOPMENT OF GOLD NANOPARTICLE-BASED PLASMONIC ASSAY PLATFORM FOR *Escherichia coli* DETECTION

A Thesis Submitted to
the Graduate School of Engineering and Sciences of
Izmir Institute of Technology
in Partial Fulfillment of the Requirements for the Degree of

MASTER OF SCIENCE

in Biotechnology

by
Duygu ERDOĞAN

July, 2017
IZMIR

We approve the thesis of **Duygu ERDOĞAN**

Examining Committee Members:

_____
Asst. Prof. Dr. Ahu ARSLAN YILDIZ
Department of Bioengineering, Izmir Institute of Technology

_____
Asst. Prof. Dr. Nur Başak SÜRMELİ
Department of Bioengineering, Izmir Institute of Technology

_____
Asst. Prof. Dr. Evren KOBAN BAŞTANLAR
Department of Biology, Ege University

24 July 2017

_____
Asst. Prof. Dr. Ahu ARSLAN YILDIZ
Supervisor,
Department of Bioengineering
Izmir Institute of Technology

_____
Asst. Prof. Dr. Ümit Hakan YILDIZ
Co-Supervisor,
Department of Chemistry
Izmir Institute of Technology

_____
Assoc. Prof. Dr. Engin ÖZÇİVİCİ
Head of the Department of
Biotechnology and Bioengineering

_____
Prof. Dr. Aysun SOFUOĞLU
Dean of the Graduate School of
Engineering and Sciences

ACKNOWLEDGEMENT

First of all, I would like to thank my thesis supervisor Asst. Prof. Dr. Ahu Arslan Yıldız and co-supervisor Asst. Prof. Dr. Ümit Hakan Yıldız for their guidance, suggestions, patience, encouragement and support throughout my thesis study.

I would like to thank Assoc. Prof. Dr. Yalın Baştanlar and his student Bahadır Mezgil for their collaborated work in the part of characterization step and Asst. Prof. Dr. Nur Başak Sürmeli for providing the bacteria that I use in my experiments.

In addition, I also thank to the specialists at IZTECH-Center of Materials Research for the SEM and AFM analysis.

Besides, I would like to thank all members of the Biomimetics and BioSens & BioApps groups for their friendship and for their aids in any case, especially Nida Demirçak for her suggestions at bacterial experiment.

I am very grateful to my lovely friends Esra Türker, Cemre Yaşar, Derya Aslan, Çağatay Sarıtepe, Mustafa Umut Mutlu, Müge Yücel, Sezer Özenler, Gürcan Şakar, especially to Yeşim Alduran for her aid at the my experiments, Anıl İncel for his suggestions about gold synthesis and also to my other friends whom I can not write their name. They helped me when I need. They have listened to me without being tired and always support me and encouragement me in any cases. We had good times together and I wish them successful and happy tomorrows.

Finally, I would like to offer my special thanks to my family for their love, always trusting, supporting and encouraging me in every moment of my life. I am very lucky to have such a great family. I love them so much and dedicate my thesis to my family, especially to my parents.

ABSTRACT

DEVELOPMENT OF GOLD NANOPARTICLE-BASED PLASMONIC ASSAY PLATFORM FOR *Escherichia coli* DETECTION

The traditional methods for pathogen detection have long detection time and insufficient sensitivity. Optical methods can overcome these drawbacks. There are solution based nanoparticle growth in the literature to enhance a surface sensitivity for biosensing applications. In this project, surface refractive index (RI) sensitivity was enhanced on solid support via gold growth to develop a label free, simple and cost-effective methodology for bacteria screening. The gold nanoparticles (GNPs) were grown on solid support by using 20 µl of $HAuCl_4$ / 80 µl of NH2OH at varied incubation times. Firstly, about 20 nm GNPs were synthesized and immobilized on polystyrene surfaces. Then, these GNPs were utilized as seed particles, and grown on solid support. During GNPs growth, a red shift in the plasmonic wavelength was observed. Morphological characterization showed that almost uniform gold growth could be achieved. The plasmonic platform sensitivity was validated by varied concentrations of sucrose, ethanol and BSA solutions, showing that the plasmonic platform gave a response to any small RI change. Next, two different *E.coli* bacterial strains' adsorption was tested. Adsorption screenings for about 10^7 *E.coli* DH5-alpha cells/ml and 10^7 *E.coli* BL21(DE3) cells/ml in Phosphate Buffer Saline were made on growth gold surfaces. Further, *E.coli* BL21(DE3) containing milk and apple juice were also adsorbed on these gold surfaces with a 30 min incubation time. The results showed that these gold surfaces exhibit higher binding kinetics for bacteria. Therefore, the proposed LSPR-based label free methodology can be an alternative to the bacteria screening in water or food samples.

ÖZET

Escherichia coli TAYİNİ İÇİN ALTIN NANOPARÇACIK TEMELLİ PLAZMONİK DENEY PLATFORMU GELİŞTİRME

Bakteri tayini için kullanılan geleneksel metotlar yeterli duyarlılığa sahip değildir ve uzun tayin süreleri gerektirir. Optik metotlar bu dezavantajların üstesinden gelebilmektedir. Literatüre bakıldığında, biyoalgılama uygulamalarında, yüzey duyarlılığını arttırmak için, yüzeydeki nanopartiküllerin büyütüldüğü ve büyütmenin de yüzeyin büyüme solüsyonuna daldırılması ile yapıldığı görülmektedir. Bu projede ise, yüzeyin refraktif indeks (RI) duyarlılığının arttırılması katı yüzey üzerinde altın büyütülmesi ile sağlanmıştır ve bakteri varlığının tespiti için etiketsiz,kolay ve ucuz yeni bir metodoloji geliştirilmesi hedeflenmiştir. Altın nanopartiküller (ANP'ler) katı yüzey üzerinde 20 µl $HAuCl_4$ / 80 µl NH_2OH kullanılarak, zamana bağlı olarak büyütülmüştür. İlk olarak, 20 nm civarında ANP'ler sentezlenmiştir. Kolloidal ANP'ler polisitiren yüzeyler üzerinde immobilize edilmiş ve daha sonrasında partiküller yüzeyde büyütülmüştür. ANP'lerin büyümesi sırasında plazmonik dalga boyunda kırmızıya kayma gözlemlenmiştir. Parçacıkların katı yüzeyde neredeyse homojen immobilizasyonu ve büyümesi morfolojik karakterizasyon ile desteklenmiştir. Plazmonik platformun duyarlılığı, değişen konsantrasyonlarda sükroz, etanol ve BSA solüsyonları kullanılarak valide edilmiş ve plazmonik platformun çok küçük RI değişimlerine tepki verdiği gösterilmiştir. Son olarak, büyütülen altın parçacıkları üzerine *E.coli* bakterileri adsorbe edilmiştir. Yaklaşık 10^7 hücre/ml olan *E.coli* DH5-alfa ve *E.coli* BL21 (DE3) içeren fosfat tampon çözeltisi ve *E.coli* BL21(DE3) içeren süt ve elma suyu, büyütülen altın yüzey üzerinde adsorbe edilmiştir. Sonuçlar, bakterilerin artan altın boyutuna paralel olarak bağlanma kinetiğinin de arttığını göstermektedir. Önerilen LSPR-tabanlı etiketsiz metodoloji, su veya gıda örneklerindeki bakteri varlığı tespiti için alternatif olabilir.

TABLE OF CONTENTS

LIST OF FIGURES

LIST OF TABLES

Table **Page**

CHAPTER 1

INTRODUCTION

1.1. Scope of the Thesis

The immobilized gold nanoparticles on polystyrene solid supports were subjected to grow by strong and mild reducing agents enabling to control shift in the plasmonic wavelength. The plasmonic substrates have found to be sensitive to marginal changes in refractive index of medium depending on the growth rate of immobilized gold nanoparticles. The plasmonic surface that exhibits significant refractive index sensitivity was utilized to the *E. coli* bacteria strains screening.

The first chapter gives fundamental information and a literature reviews. The second chapter summarizes the theoretical background about characterization methods. Experimental section is given in chapter 3, and results with discussion explained in chapter 4. The chapter 5 concludes the thesis.

1.2. Nanoparticles

Particles ranging from 1 to 100 nm are called as nanoparticles (NPs). They can be produced from a variety of chemical materials, including the common metals, metal oxides, non-oxidized ceramics, silicates, polymers, organics, carbon and biomolecules.[1] Recently, nanoparticles gained a great attraction compared to bulk materials since their physical properties like electronic, mechanic, optic etc. and chemical properties rely on their size and structure. Therefore, the materials may be prepared with the desired properties.[2] NPs have good surface characteristics that are suitable for chemical modification, have good biocompatibility and large surface area/volume ratio. Thus, they can be used as signal transducers and nano-transporters, as well as they can be used in preparation of analyte conjugating or catching probes, etc.[3] The metal NPs' surface can be functionalized specifically using biomolecules for imaging, treatment and

detection purposes. They are used for bioimaging, biosensing, photothermic and photodynamic therapy, drug and gene transportation.[4]

1.2.1. Metal Nanoparticles' Property: Localized Surface Plasmon Resonance

Metal NPs produce enhanced electromagnetic fields affecting the local environment. They have free electrons in d orbital which can travel freely through the material. Thus, scattering from the bulk is not expected in such smaller particles and it is assumed that all interactions are on the surface.[5] As shown in Figure 1.1, when a metal particle's surface is irradiated with electromagnetic radiation at appropriate frequency, the coherent emission of electrons in the metal is induced perpendicular to the direction of light propagation. When metallic NPs are smaller than the wavelength of incoming light, electron cloud oscillation named as 'plasmon' is localized on the NPs' surface. This phenomenon is called localized surface plasmon resonance (**LSPR**).[6-7]

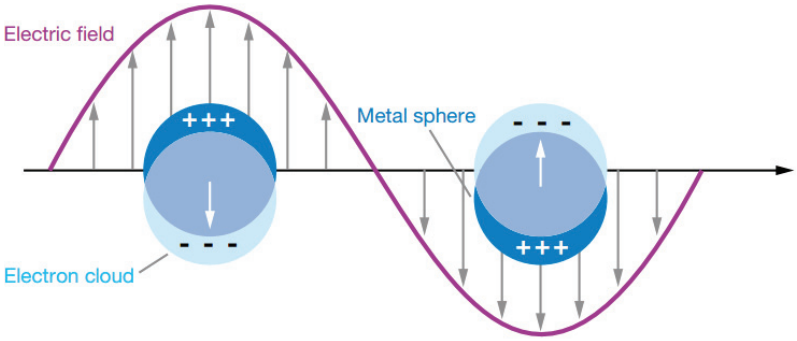

Figure 1.1. Schematic illustrating of a localized surface plasmon[7]

The plasmon resonance frequency of electron vibrations is very dependent on the nature of the metal NPs' properties like their size (Figure 1.2.a), structure, material, composition and as well of the distance between the individual nanoparticles and this provides spectral adjustability of plasmon resonance over the entire visible and near infrared ranges. The dielectric adjacent environment has also important role in the LSPR frequency and this provides to detect small refractive index (RI) changes near the nanostructures.[8] The Figure 1.2.b demonstrates the frequency of LSPR showing a red shift with an increase in the RI of the medium. The specific analyte binding to NPs generates the RI variation causing the plasmon band shift and enables an immense

usage as an optical sensing medium.[9] The local electromagnetic field that occurs near the NP larger than the incident fields in orders of magnitude, and near the resonance peak wavelength scattering is very powerful. For biomolecular manipulation, labeling, and detection, it has been proven that this local area enhancement and powerful scattering are very special.[10]

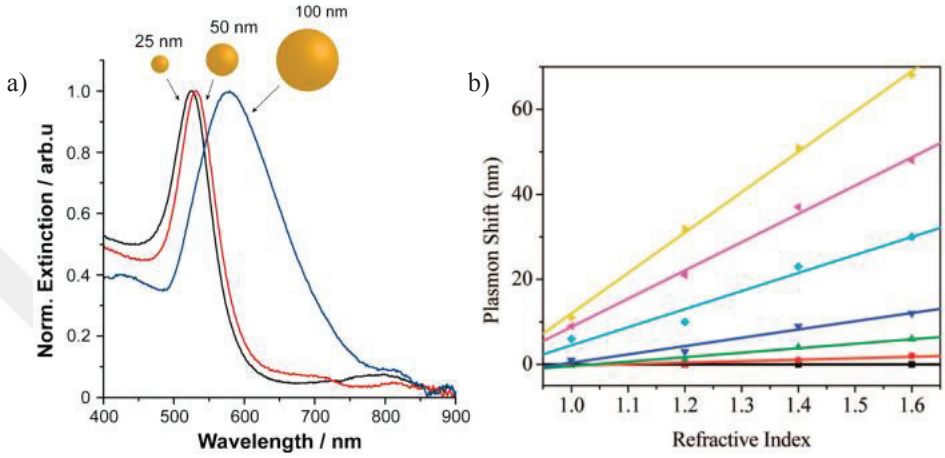

Figure 1.2. a) Extinction spectra for GNPs in water[8] b) plasmon shift for a pair of 40 nm GNPs as a function of refractive index of medium for different interparticle separations[9]

Gold (Au) and silver (Ag) are usually preferred metallic nanoparticles because of their simple preparations, relatively high stability, unique optical properties, and the ability to form strong electrostatic conjugation with biomolecules.[3] However, when considered the chemical stability, Au has lower oxidation rate than Ag so it makes the gold more favorable metal nanoparticle in plasmonic application.

1.3. Gold Nanoparticles

The use of Gold Nanoparticles (GNPs) has been increasing in recent days because of their favorable optical properties, biocompatibility and bioconjugation ability.[11] The main advantages are easy synthesis by chemical reduction methods and having a low toxicity compared to various nanomaterials.[12] The nano-scale properties of GNPs depend on size and structure. Therefore a comprehensive effort is needed to

control the size, shape and surface composition of them while keeping narrow size distributions at the same time.[13]

GNPs show a large coefficient of extinction due to LSPR that is the source of the gold colloids' color.[14] The isolated GNPs solution at about 520 nm has red shift in max plasmon wavelength when they are assembled or aggregated, and a change occurs in visible color from purple to red.[15] Their plasmon resonance is detected up to 3 nm diameters. Thus, over this size, enhanced electromagnetic field arises at the gold surface; therefore spectroscopic techniques can be used to obtain surface-enhanced optical properties. Depending on the GNPs' size and structure, GNPs has both scattering and absorption characteristic at different ratio. GNPs less than 20 nm exhibit absorption substantially, but if size increased up to 80 nm, the rate of scattering increases.[16]

1.3.1. Gold Nanoparticle Synthesis

A variety of strategies have been developed for the GNPs synthesis to produce sphere, rod, triangle, cube and star structures.[8] The general accepted idea is that the concentration of Au atom after reducing from $AuCl_4^-$ increases rapidly up to supersaturation level firstly. A sudden explosion of nuclei generation (nucleation step) occurs from the Au atoms collision and finally, attaching of other gold atoms to nuclei provide growing.[17]

There are two approaches called as 'top down' and 'bottom up' to synthesize GNPs as summarized in Figure 1.3.[18] The first approach, physical technique, is the breaking up bulk metal, than they are synthesized from gold ions. Several methods have been utilized to make the particles from gold ions such as; chemical[19], photochemical[20], sonochemical[21-22], electrochemical[23], irradiation[24], laser ablation[25-26] etc.[27] However, most of them start with Au^{3+} ions and produce particles with varied sizes using different reductants.[28] In latter approach, chemical reduction technique, there are two stages as nucleation and consecutive growth. When the two steps are accomplished in the same process, this is called in situ synthesis; otherwise this is called the seed growth method. In situ synthesized GNPs can also be utilized for seed growth or other functionalization strategies. In addition, there are two main steps to prepare GNPs by chemical reduction. The first step includes a reducing agent; which can be borohydrides, formaldehyde,

aminoboranes, hydrazine, hydroxylamine, alcohols, sugars, carbon monoxide, hydrogen peroxide, sulfites, citric and oxalic acids etc. The second step includes a stabilizing agent; which can be dendrimers, polymers, sulfur containing ligands (especially thiolates), nitrogen-based ligands, phosphorus ligands, oxygen-based ligands, trisodium citrate dihydrate and surfactant (particularly CTAB, stands for cetyltrimethylammonium bromide).[29] One chemical; namely trisodium citrate can act as both reducing and stabilizing agent.[30]

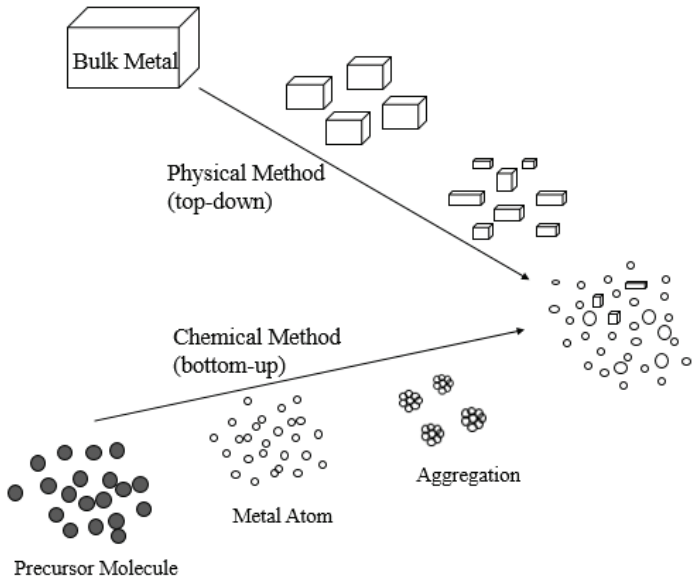

Figure 1.3. Schematic illustration of metal nanoparticles preparation[18]

The first study about the GNPs synthesis from reduction of $AuCl_4$ with phosphorus was made by Faraday.[31] Then, Turkevich method is developed in 1951 [30] in which citrate is used as the reducing and the stabilizing agent to prepare GNPs in hot aqueous solution and this method was improved by Frens in 1973.[32] Next, Au_{55}-phosphine cluster as stabilizer was used by Schmid in 1981. Then thiolates were utilized for GNPs' synthesis and stabilization by Mulvaney and Giersing in 1993.[29] Lastly, alkane thiols (as stabilizer) with sodium borohydride (as reducing agent) were used in the Brust-Schiffrin method in 1994. There is a common observation in these methods that the size of the particle depends on the ratio between gold salt and reducing agent, and also the adsorption rate of stabilizer effects the particle size.[33] Among these methods, the Turkevich method is still one of the most commonly utilized procedures to give 15-20 nm colloids. On the other hand, to synthesize various sizes of GNPs Brust

method can be utilized to produce 1-3 nm of gold particles, and size of the particles can be adjusted between 2 and 5 nm.[27]

1.3.1.1. Turkevich Method

Turkevich et al. (1951) used citrate as both the reducing and the stabilizing agent to synthesize GNPs [30], and this method was one of the heavily used methodology for in situ GNPs synthesis. It includes rapid addition of trisodium citrate dihydrate into boiled $HAuCl_4$ solution, and the reaction continues till wine red colloidal suspension occurs in which the size of the each particle is around 20 nm. The reaction between auric chloride and trisodium citrate is illustrated in Figure 1.4. On the other hand, Frens showed that synthesized GNPs varies from 15 to 150 nm by adjusting the citrate to gold ratio.[29] Citrate can also be used only as stabilizing agent. For example, tannic acid and citrate mixture was used to synthesize about 3 to 17 nm GNPs at 60 °C.[34] Another example that 6 nm GNPs were synthesized at room temperature while utilizing citrate as the stabilizer and $NaBH_4$ as the reducing agent.[35]

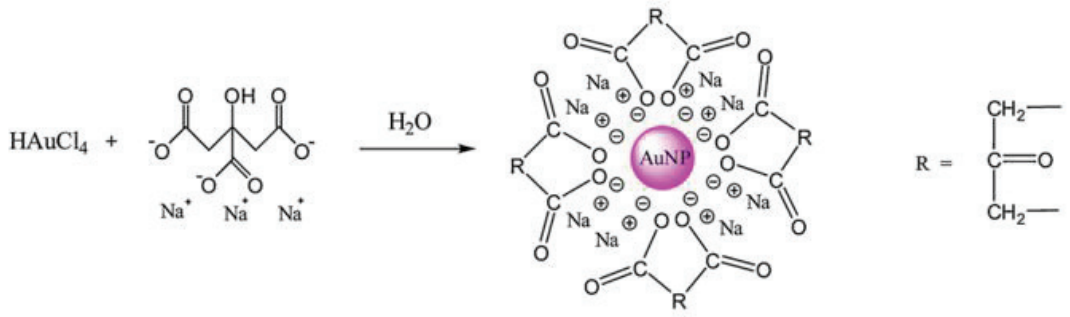

Figure 1.4. The Turkevich method GNP synthesis[29]

Kumar et al.[33] developed a model that trisodium citrate oxidation to dicarboxy acetone provides the Au^+ reduction from Au^{3+}. After decomposing dicarboxy acetone at the experimental temperature, the gold atoms are formed by disproportionation of Au^+ on the gold surface. This reaction leads to the formation and growth of the nuclei. Therefore, they showed that citrate does not just act as both reducing and stabilizing agent, but also it causes to the degradation of the intermediate product.[33]

1.3.1.2. Brust-Schiffrin Method

The two-phase Brust-Schiffrin technique[36] uses thiolate stabilizer to synthesize GNPs in the size range of 2 to 5 nm. It provides easy preparation at ambient conditions, thermal stability of the particles, relatively easy functionalization and modification with ligand substitution etc. The cuboctahedral and icosahedral structures of GNPs are stabilized via Au-S bonds. Larger ratios of S/Au yield smaller core sizes based on the "nucleation-growth-passivation kinetics" model in which sulfur containing agents suppress the growth process. In addition, the smaller and monodispersed GNPs are also synthesized by rapid $NaBH_4$ addition in cold solution.[29]

Moreover, Brust et al.[36] grew metal clusters by attaching self-assembled thiol monolayer onto growing nuclei simultaneously. So a two-phase system (water/toluene) was used to grow the particles during nucleation. For this case, $AuCl_4^-$ was reduced with sodium borohydride in an alkanethiol (dodecanethiol, $C_{12}H_{25}SH$) after phase transfer to toluene from aqueous solution by using tetraoctylammonium bromide. Finally, a surface was coated with thiol which contains 1-3 nm Au particles.

1.3.1.3. Schmid's Au_{55} Cluster and the Phosphorus Ligands

Phosphine-stabilized gold clusters were prepared by Au^{3+} reduction with diborane in $P(C_6H_5)_3$ presence in 1981 by Schmid et al.[37] to obtain cluster of gold formulated as $Au_{55}[P(C_6H_5)_3]_{12}Cl_6$. Schmid's Au_{55} cluster is likely the most well-known ligand which stabilizes the metal nanoparticle. This method yields small, highly homogeneous GNPs that has the structure of Au_{55} mostly.[18]

Schmid's method was further developed by Weare et al.[38] in 2000 by using $HAuCl_4$ and $N(C_8H_{15})_4Br$ in a water-toluene mixture with PPh3 and, instead of diborane, NaBH4 was added. $[Au_{101}(PPh_3)_{21}Cl_5]$ cluster was produced with a impurity of $[Au(PPh_3)Cl]$. Next, $[AuCl(SMe_2)]$ complex was used as precursor gold source instead of $HAuCl_4$ and sodium naphthalenide ($C_{10}H_8Na$) was used as reducing agent instead of NaBH4 to form phosphinine-stabilized GNPs by Moores et al.[39] Later, 9-borabicyclo-[3.3.1]nonane (9-BBN) which is mild reducing agent was also utilized to synthesize 1.2–2.8 nm triphenylphosphine-stabilized GNPs.[40]

1.3.1.4. Biosynthesis and "Green Chemistry"

A natural molecule can be used directly as a reducing and stabilizing agent to produce GNPs. Natural polymers, natural extracts and microorganisms can be utilized as the sources.[29] The extracts from natural sources which has phenol, hydroxyl carbonyl and carboxyl groups reduce the Au^{3+} to stabilize GNPs. By using naturally derived extracts, GNPs synthesis is simple; the extracts are only mixed with aqueous $HAuCl_4$ until the color turns to red or purple.[29] Chitosan[41-42], which is a natural polymer, stabilizes GNPs with amine groups. GNPs are also stabilized by microorganisms[43] and so far, four major microorganisms have been used for GNPs synthesis: bacteria, fungi, yeast and actinomyces. The carboxyl groups' abundance in the microorganisms is thought to play an important role in the reduction of Au^{3+}. Furthermore, the electronegative groups such as carboxyl, thiol, amine, sulfur in the microorganisms contribute to the GNPs structure by microbial stabilization.[29]

1.3.2. Seed-Growth Method

The conventional in situ synthesis produces spherical or quasispherical GNPs but the control of GNPs' size and structure is difficult as the gold size increases. For this reason, the seed growth strategy has been shown as a very effective method for the production of monodisperse and well defined GNPs structures up to 300 nm.[29]

When compared with in-situ synthesis, the particles are enlarged progressively in the seed growth technique. This technique has been widely utilized because the method makes easier to control the GNPs' size and structure. General procedure involves formation of the small GNP seeds and then growth of Au atom on the surface of the seed particle. The gold growth occurs in growth solution which contains $HAuCl_4$ and the reducing and the stabilizing agents.[29] The nanoparticles at a narrow size range would be produced successfully by adjusting nucleation and growth steps, otherwise presence of the seed particles could create further nucleation.[44]

Natan et al.[45] synthesized the GNPs in a size range between 20 nm and 100 nm by addition of $NaBH_4$ and citrate capped Au seeds into a growth solution, which contains mild reducing agents; like citrate or hydroxylamine. However, they obtained also small amount of Au nanorods as impurities. The seed growth method is also

developed by the Murphy et al. and later by the group of El Sayed to synthesize gold nanorods (GNRs). In 2001, Murphy et al.[46] produced GNRs from 3-4 nm of citrate capped GNPs by adding the seed particles into the growth solution which contained $HAuCl_4$, ascorbic acid and CTAB. They grew the particles at multiple step by using products from previous cycle as a seed particle. However, the yield was very low due to uncontrollable amount of the other structures. On the other hand, El Sayed's group[47] were used CTAB instead of citrate during the Au seed formation and silver nitrate as a reducing agent during the Au seed growth resulting very high yield GNP synthesis.[29]

The GNPs were also produced by dipping seeded Au surface in the growth solution contained NH_2OH/Au^{3+} solution.[28, 45, 48-49] 23 nm of GNPs were grown up to 32 nm at room temperature for 2 minutes. Au ions had been reduced on the GNPs surface which causes coupling effect resulting from increasing diameter of the particles and decreasing the distance between the particles.[48] The NH_2OH reduces the Au particles thermodynamically at the surface and causes enlargement of gold particles at the gold surface in the solution instead of a new gold nucleation starting. Thus, these properties make NH_2OH/Au^{3+} seeding a useful tool for the production of colloidal Au-based materials at the desired size.[49]

1.4. Plasmonic Biosensing

Optical nanobiosensors have been used for medical diagnosis, diseases screening, drug discovery, biological agents and environmental pollutants detection etc.[50] Current methods for detection and sensing are powerful, but they have insufficient sensitivity, long process times and label requirement, high costs etc. On the other hand, optical spectroscopic methods have the advantage of being fast, noncontact and relatively cost effective, but they are not necessarily sufficiently sensitive.[51] Different strategies can be used to increase the plasmonic nanosensors' sensitivity. As illustrated in Figure 1.5, there are various methods to influence the dielectric properties of the environment of plasmonic nanoparticles motivated by nanoparticle characteristics, enhancement schemes and plasmon coupling etc.[52]

The peak wavelength, λ_{max}, depends on the nanoparticle size, shape, composition, orientation and local dielectric environment. Looking at the LSPR shift is a general technique used to measure any molecular binding affinity that alter the local

refractive index. Specificity for known analytes is obtained by using molecular recognition elements such as antibodies and blocking agents, by specific dye or specific analyte.[53]

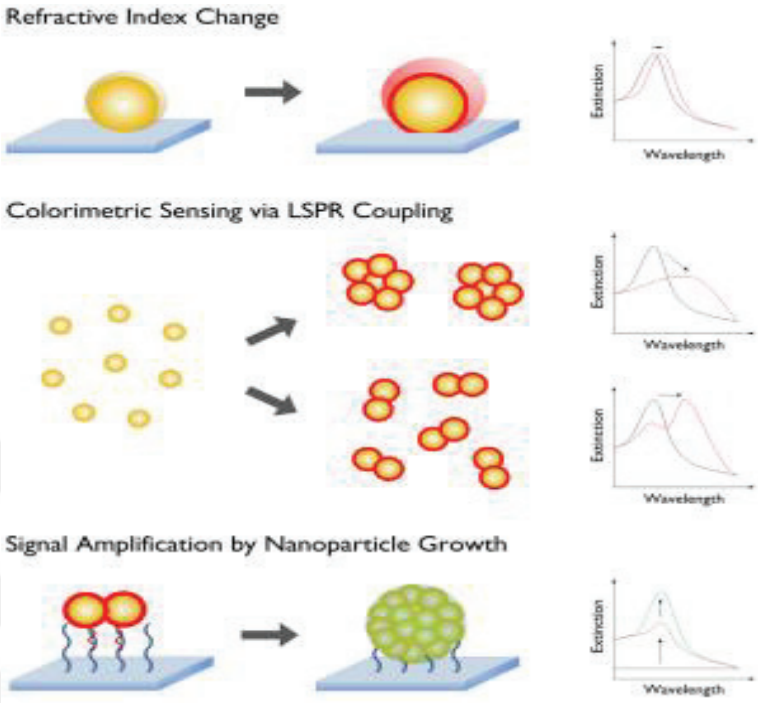

Figure 1.5. Different strategies to increase the plasmonic nanosensors' sensitivity[52]

1.5. Bacteria Screening

The bacterial cell wall and membrane play a critical role in organizing the significant bacterial functions of attachment, disintegration, motility, cellular differentiation etc.[54] In both Gram-positive and Gram-negative bacteria, the cell wall is formed from a polymer peptidoglycan which is a glycan composition cross-linked with tensible peptides and protect cell from lysis.[54]

The pathogenic bacteria detection has crucial importance in food industry and in water reservoir monitoring. The present detection methods are currently based on traditional cultivation of bacterial pathogens which are standardized protocols.[55] The other conventional methods are based on immunological techniques such as enzyme linked immunosorbent assay (ELISA), and polymerase chain reaction (PCR). These methods give high precision and reliability, providing qualitative and quantitative information. On the other hand, they require long process time and trained personal.[56]

Therefore, alternative methods are required to detect pathogens in the contaminated environment with high sensitivity, short detection time, and simplicity. Recently, much interest has been paid to the unlabeled detection methods which are based on biosensors.[55]

An electrochemical biosensor was used to detect *E. coli* O157:H7 by using antibody-modified nanoparticles. In the experiment, while polymer covered magnetic nanoparticles were utilized to separate target bacteria, carbohydrate-capped GNPs were used to label the target. At the end, the bacteria were detected by an electrochemical signal. The all reaction was completed only at 45 minutes which offers rapid detection. In addition, the dynamic range of limit of detection is at 10^1 to 10^6 cfu/ml.[57]

Salmonella, which is pathogenic microorganism, was detected by Surface Plasmon Resonance (SPR) immunosensor platform with the help of self-assembled protein G binding to the gold surface and 2-iminothiolane, -SH group. A commercial Mab against *S. paratyphi* was also used to detect *S. paratyphi*. Additionally, indirect ELISA was performed to examine the cross-reaction between the Mab against *S. paratyphi* and related pathogens which exist in contaminated water. Therefore, it was showed that the SPR shift depends on the specific binding of target bacteria is higher for *S. paratyphi.* In this technique, the detection limit was 10^2 cfu/ml which was four orders of magnitude more sensitive than a classical ELISA.[58]

In another example, an agarose based microfluidic concentrator was coupled to an immunofluorescence system to diagnose pathogens. *E. coli* DH5 alpha, *E. coli* OP50, and *S. aureus* were chosen as a model. Rabbit Anti-E.coli DH5 alpha/FITC and Rabbit Anti-Staphylococcus Enterotoxin B/FITC were used to functionalize the microchannels. Validation of the device was made with plasma and urine samples. As a result, high recovery yield (over 90%) and high performance were obtained for *S. aureus* detection in a patient plasma.[59]

The large existence of lipopolysaccharides (LPS) is an indication of bacterial contamination as well. The GNPs usage may be a potential and easy way to detect LPS as a colorimetric test. Sun et al.[60] used the 35 nm cysteamine-modified cationic GNPs, and investigated the interaction between cationic nanoparticles and LPS on *E. coli* (10^8 cfu/mL) surface. They showed that LPS on *E. coli* cells surface can interact with cationic nanoparticles which causes aggregation and color change, so a rapid and easy assay has been developed for visual LPS detection.

Compared to traditional methods for pathogen detection, functionalized GNPs provide a colorimetric output that is generally visible by the naked eye. However, the most important constraint of this strategy is that, the various interferents in the medium can lead to the non-specific accumulation of nanoparticles and thus produces a false positive signal. The colorimetric response obtained from nanoparticles via aggregation may have insufficient sensitivity therefore signal amplification via gold or silver growing can be used.[56] For example, Li et al.[61] has been developed a strategy to detect protozoa and bacteria. They captured the target cells by antibody-functionalized GNPs and then they were transferred the cells to the gold growth solution after discarding free Au immunoprobes. Detectable color development quantitatively was obtained from the catalytic growth of GNPs. *G. lamblia cysts* detection limit was determined as low as $1.088 * 10^3$ cells/ml.

CHAPTER 2

CHARACTERIZATION METHODS

In this project, GNPs were synthesized and immobilized onto a solid support. After immobilization, the GNPs were grown directly on the surface to enhance RI sensitivity. Finally, overnight-cultured two bacteria strains were being screened on the developed plasmonic platform without any labelling. The following section will give a brief theoretical information about the characterization techniques, which were used in this project.

2.1. Zeta-Sizer

Particle size, zeta potential and molecular weight that are basic parameters for characterization of a particle, can be measured at a wide range by using Zeta-sizer system. The Zeta-sizer Nano series are equipped with a 633 nm red laser or a 532 nm green laser and at 173° or 90° with detector position. The instrument uses the Dynamic Light Scattering (DLS) technique which its working principle is shown in Figure 2.1. to measure the size of the particles. DLS, which is also known as Photon Correlation Spectroscopy, correlates the particles size via measuring Brownian motion (Stokes-Einstein equation). The system calculates the size by measuring fluctuations in the scattered light intensity.[62]

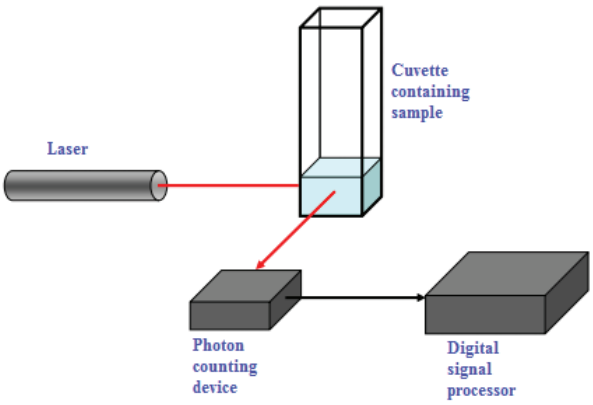

Figure 2.1. Schematic of DLS setup[63]

2.2. Ultraviolet -Visible Spectrophotometry

Spectrophotometry which its general working principle is demonstrated in Figure 2.2. is a scientific technique depends on the absorption of light by a matter illustrated. Absorption is the amount of light which a substance absorbs and does not let it to pass through it.[64]

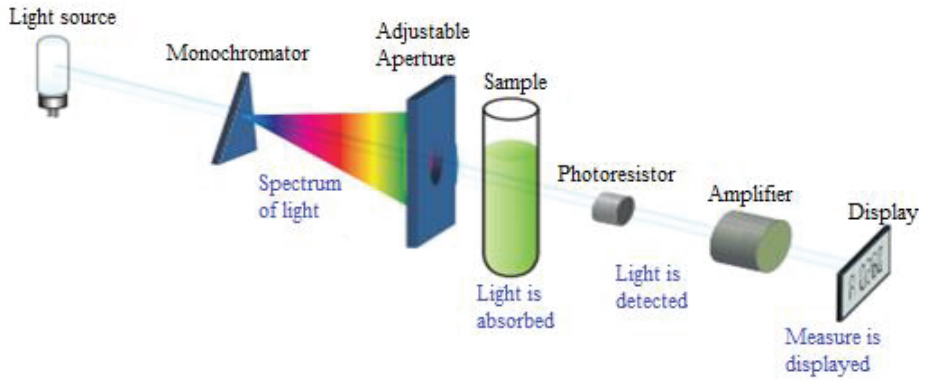

Figure 2.2. General illustration of a spectrophotometer[64]

The Ultraviolet-Visible (UV-VIS) spectrophotometer is an instrument that measures the intensity ratio of two beams of light in the UV-VIS region. This technique is simple, fast, moderately specific and can be applied to compounds in small quantities. Quantitative spectrophotometric analysis utilizes the fundamental Beer-Lambert law.[65] While Lambert's law which says the light source independence with absorption[64] relates the beam intensity of parallel monochromatic light to medium thickness, Beer's law relates absorbance to concentration.[65] When combined the two laws:

$$\text{Beer-Lambert law: } A = abc \qquad (2.1)$$

Where 'A' states absorbance or optical density, 'a' states absorptivity or extinction coefficient, 'b' states path length of radiation through sample (cm) and 'c' states solute concentration in solution. Both 'a' and 'b' are constant so absorbance is directly proportional to the concentration. [65]

Measurements can be made with:[64] a) Single wavelength is an absorption measurement at a single constant wavelength such as 260 nm for DNA. b) Wavelength scan is an absorption measurement at wavelengths range, spectrum of absorbance against wavelength. c) Kinetic is an absorption measurement at a single wavelength

with time intervals, plot of absorption against time, to reaction progress measurement. d) Cell Density is an absorption measurement at 600 nm with time intervals, possibility to determine bacterial cell concentration and to determine harvesting time for the culture. e) Quantitative analysis is an absorption measurement at a single wavelength of a number of known standards, to determine unknown samples by using standard curve.

2.3. Scanning Electron Microscopy (SEM)

Scanning Electron Microscopy (SEM) can give an idea about surface topography, crystal structure, chemical composition, and the electrical behavior of the sample. The surface to be analyzed is immobilized to electrically conductive pads on special SEM stub. If the sample is immobilized on an insulator, a conduction path to base is needed to prevent the sample charging (the image distortion).[66] In SEM, a fine electrons probe, typically with energies up to 40 keV, is focused on a sample and scanned along a pattern of parallel lines.[67]

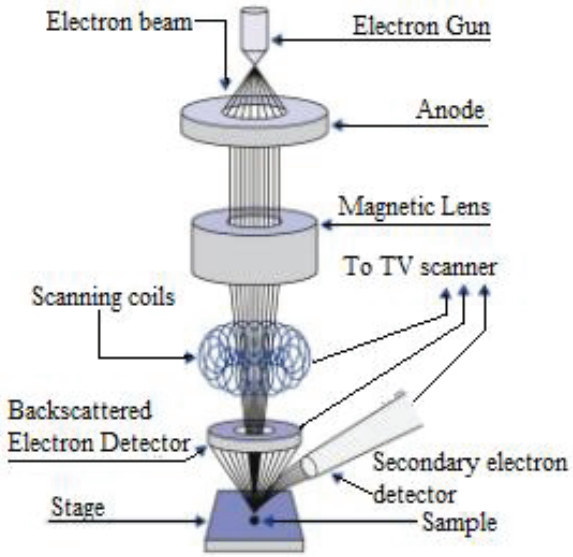

Figure 2.3. SEM principle design[68]

Two or three electromagnetic condenser lenses demagnetize the electron beam. The electrons in which their dimension depends on the electron beam energy, elemental atomic masses in the sample and collision angle of the electron beam to the sample.[66] The various signals are generated due to incident electrons collision collected to analyze

the surface of the sample or to generate an image. These are mostly secondary electrons, with a few tens of eV energies, backscattered high energy electrons, and characteristic X-rays.[67] The signal from each detector can be sent to a rasterized monitor in synchronism with the electron beam. The image magnification is determined via the ratio of the monitor screen side length to the raster side length on the sample.[66] The SEM principle design[68] is demonstrated in Figure 2.3.

2.4. Atomic Force Microscopy (AFM)

The AFM working principle is to scan the surface of the sample with feedback mechanisms by the tip that allow the end of the piezoelectric scanners to hold a constant force or a fixed height above the surface of the sample. When the tip scans the sample surface, it moves up and down with the surface shape and the laser beam deviations from the cantilever measures the differences in light intensity between the top and bottom photodetectors. The feedback from the photodiode signal distinction allows the tip to maintain an unchanged force or an unchanged height over the sample due to the computer software control. While piezoelectric transducer is monitoring real time height deviation in the mode of constant force, the force of deviations on the sample is reported in a mode of constant height. There are typically three operation modes of micro-cantilever systems and these are non-contact, contact and tapping mode.[69-71] Figure 2.4. shows the representative illustration of AFM operation process[70].

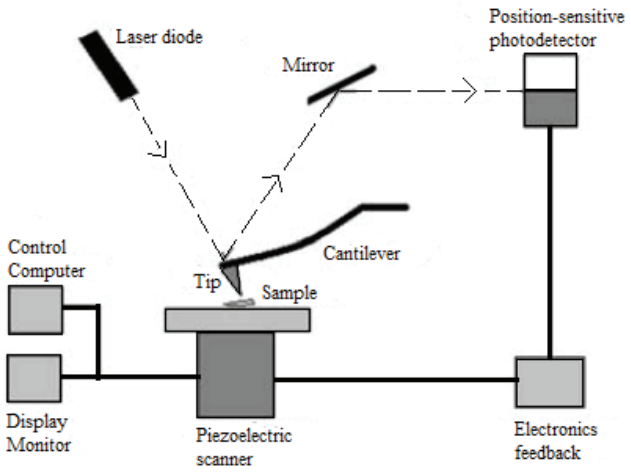

Figure 2.4. AFM operation process[70]

In contact mode, a tip attached to cantilever is kept a contact with the sample surface. Therefore, it applies a much greater force to the sample and sometimes causes poor images and soft samples to be distorted by the tip. In non-contact mode, the cantilever is oscillated slightly above the resonance frequency of the cantilever, typically a few nanometers (<10 nm). In the other, tapping, mode, a tip attached to oscillating cantilever contacts the surface intermittently at the lowest point of the oscillation. Thus, this mode significantly reduces the forces applied by the tip on the sample as compared to the contact mode and decreases both the tip and sample damage.[70]

2.5. Artificial Neural Network (ANN)

An Artificial Neural Network (ANN) is a mathematical model that mimics human neuron architecture which has the ability of leaning and generalizing. ANN is constructed by a number of "neurons" (or "nodes") with an "input", one or more "hidden" and an "output" layers. Each neuron in the layer is connected to each neuron in the next layer via a weighted connection (the weight indicates the connection strength).[72] The mostly used neural network learning method is back-propagation for artificial neural networks training. The algorithm for the optimum weight searching works in accordance with the rules of the gradient.[73] In a simple ANN, input data are passed into hidden layer which involves simple mathematical calculations via the weight of links and input values. The results are given to a non-linear mathematical function (for instance a sigmoid function) and the final outputs are generated. The output values are input to the next layer and the calculation operations are repeated for the remaining layers, finally resulting in output values of the network.[74] Principle Component Analysis (PCA) is a statistical method which transforms correlated variables' set into uncorrelated variables' set by decreasing dimension of data with minimum loss. Applying PCA on the data before feeding an ANN provides faster analysis by problem's complexity reduction via shortening dataset dimensionality.[75]

CHAPTER 3

EXPERIMENTAL SECTION

3.1. Materials & Methods

Polystyrene plates (tissue cultured PS plate, a flat bottom, 96-well plate) was purchased from Corning, Costar. Hydrogen tetrachloroaurate (III) hydrate ($HAuCl_4$, 99.999% trace metals basis), sodium citrate tribasic dihydrate ($Na_3C_6H_5O_7$,≥99.0%), Poly-L-lysine hydrobromide (PLL; molecular weight of 70,000-150,000), $NH_2OH{\cdot}HCl$ (NH_2OH, ACS reagent, 98.0%), L-Ascorbic acid (reagent grade, crystalline) were used as purchased from Sigma Aldrich. Sucrose (ultrapure grade) was obtained Amresco, ethanol (%99.5 v/v, Tekkim) and BSA (albumin from bovine serum, ≥96%, Sigma) were used as purchased. MilliQ water (MQ, 18.2 MΩ.cm at 25 °C, Millipore) was utilized to prepare the all solutions. *E. coli* DH5-alpha and *E. coli* BL21(DE3) bacterial strains in LB Broth was a kind gift from Dr. Nur Başak Sürmeli. LB Broth (liquid, with sodium chloride and peptones, casein ingredients) was purchased from Amresco used for the propagation and maintenance the bacteria. 10X Phosphate Buffer Solution (PBS) was purchased from Thermo Fisher but 1X PBS, with dilution, was used as solvent for BSA preparation and for bacteria experiment. The whole experiments were performed at room temperature.

Malvern Nanosight ZS was used for size determination of Au nanoparticles. The absorbance spectra was recorded by Microplate Spectrophotometer (Thermo Multiscan Go). Morphological characterization of substrates were performed by Scanning Electron Microscopy (SEM, FEI QUANTA 250 FEG) and Atomic Force Microscopy (AFM, Digital Instrument-MMSPM Nanoscope IV).

3.2. Gold Nanoparticles Synthesis in Solution

Gold nanoparticles (GNPs) were synthesized by using Turkevic method.[30] Briefly, a 0,010 g of $HAuCl_4$ was weighed and placed into a 100 mL erlenmeyer flask.

Then, it was dissolved in 60 ml of MQ water to obtain 0,5 mM $HAuCl_4$ solution which has light yellow color. This solution was stirred at 100 ^oC. In following step 0,069g of sodium citrate in 6 ml MQ (38,8 mM) was added in to solution and colorless solution was observed. The heating process was kept until the solution reached the reddish color. The temperature of the reaction medium was kept at 75 °C at final step (under 86 °C). The gold nanoparticle solution was stored at 4 °C after allowing the colloid suspension cool to room temperature. The reagents' concentration for gold synthesis was shown in Table 3.1.

Table 3.1. Concentration of reagent for nanoparticle synthesis.

Reagents for gold synthesis	Concentration
$HAuCl_4$	0,5 mM
Na_3Ctr	38,8 mM

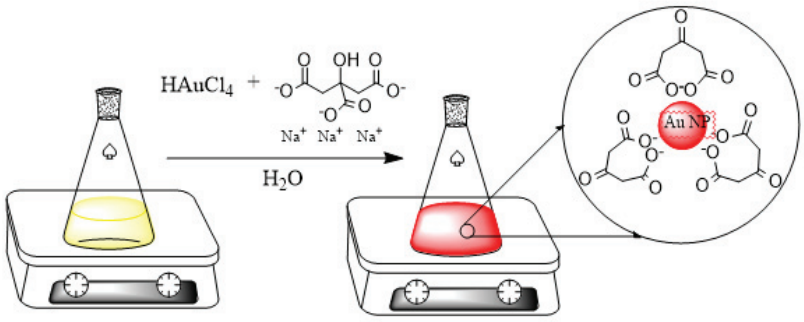

Figure 3.1. Schematic illustration of gold nanoparticle synthesis

3.3. Immobilization of Gold Seed on Solid Support

5 ml MQ water was added into a bottle contained 5 mg Poly-L-Lysine hydrobromide (PLL) (1 mg/ml stock polymer solution). Then, 1 ml PLL solution was taken into a 20 ml vial and diluted to 0,05 mg/ml PLL solution by PBS. After that, 100 µL of 50 ppm PLL in PBS was loaded onto tissue culture polystyrene surfaces which. Then, 50 µL citrate capped GNPs solution diluted 1:1 with MQ was added. The incubation time for each step was 24 hours and after each step the wells were washed with MQ water three times. The absorbance spectra of the immobilized gold surfaces

into MQ water medium were recorded by adding 100 µL for each wells. The plate was stored at + 4 °C.

3.4. Solid-state Gold Nanoparticle Growth on Gold Solid Support

The gold nanoparticle immobilized surfaces were seeded by auric chloride and reducing agents as schematically shown in Figure 3.2.

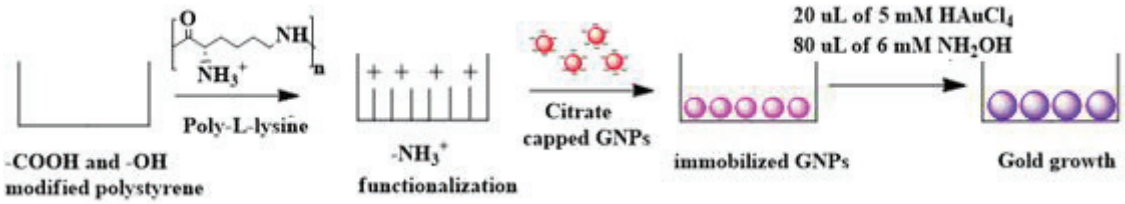

Figure 3.2. Schematic of the experimental platform

3.4.1. Gold Growth with Strong Reducing Agent, Hydroxylamine Hydrochloride

0,5 M stock $HAuCl_4$ solution was prepared first by dissolving 0,0340 g $HAuCl_4$ with 200 µL MQ into an 500 µL eppendorf. Then, 0,05 M $HAuCl_4$ solution was also prepared from 0,5 M gold solution with diluted MQ in a different 500 µL eppendorf as 500 µL as total volume. Finally, 5 mM (0,005 M) $HAuCl_4$ solution which was experimental gold concentration was prepared from 0,05 M $HAuCl_4$. After that, 0,05 M stock NH_2OH solution was prepared first by dissolving 0,0347 g NH_2OH with 10 ml MQ into a 20 ml vial. Then, 0,025 M NH_2OH solution was also prepared from 0,05 M reducing solution with diluted MQ into a different 20 ml vial as 10 ml as total volume. Finally, 6 mM (0,006 M) NH_2OH solution used as experimental reducing agent (concentration was prepared from 0,025 M NH_2OH).

First of all, the seeded gold surface spectra at 400-800 nm were recorded into 100 µL MQ water as blank to see gold growing effect at max wavelength shift. Au size growing was carried out by adding 20 µL of 5 mM $HAuCl_4$ and 80 µL of 6 mM NH_2OH to each gold surface. Growing process were performed in each minute. After discarded

growth solution at specific time onto each gold surfaces, they were washed with 300 µL MQ water three times.

3.4.1.1. Hydroxylamine Hydrochloride Concentration Optimization

2, 4, 6, 8 and 10 mM NH_2OH solution were prepared from 0,025 M NH_2OH solution respectively and used as 80 µL. Growing process were performed in each two minute as three parallel at 400-800 nm wavelength range. Up to final minutes the absorbance spectra were taken into growth solution but at final stage the surfaces were washed with 300 µL MQ water three times and the absorbance spectra of the growth gold surface were obtained in 100 µL MQ water.

Table 3.2. Concentration of reagents for gold growth onto gold solid surface

Gold precursor	Concentration		Concentration	Reducing agent
$HAuCl_4$	0,5 M	stock	0,05 M	NH_2OH
$HAuCl_4$	0,05 M	2nd stock	0,025 M	NH_2OH
$HAuCl_4$	0,005 M (5 mM)		0,002 M (2 mM)	NH_2OH
			0,004 M (4 mM)	NH_2OH
			0,006 M (6 mM)	NH_2OH
			0,008 M (8 mM)	NH_2OH
			0,01 M (10 mM)	NH_2OH

3.4.1.1.1. Growth Kinetic Studies for Hydroxylamine Hydrochloride

20 µL of 5 mM gold solution and then immediately 80 µL of 2, 4, 6, 8 and 10 mM NH_2OH solution were added onto three solid gold surface respectively. Growing process were performed in each two minute from two to twenty five minutes as three parallel while measuring their absorbance at 580, 590, 595, 600 and 605 nm. These wavelength was chosen because it considered that the max wavelength of the solid state Au growth surface was around them.

3.4.2. Growth with Mild Reducing Agent, L-Ascorbic acid

1 mM (0,001 M) $HAuCl_4$ solution which was experimental gold concentration was prepared from 5 mM $HAuCl_4$. After that, 0,05 M stock ascorbic acid solution was prepared first by dissolving 0,0088 g ascorbic acid with 1 ml MQ into an 1.5 ml eppendorf. Then, 0,025 M ascorbic acid solution was also prepared from 0,05 M reducing agent solution with diluted MQ into an different 1.5 ml eppendorf as 1 ml as total volume. Finally, 10 mM ascorbic solution was prepared from 0,025 M ascorbic solution.

First of all, the seeded gold surface spectra at 400-800 nm were recorded into 100 µL MQ water as blank to see gold growing effect at max wavelength shift. Au size growing was carried out by adding 20 µL of 1 mM $HAuCl_4$ and 80 µL of 10 mM ascorbic solution to each gold surface. Growing process were performed in each 15 minute. After discarded growth solution at specific time onto each gold surfaces, they were washed with 300 µL MQ water three times. The absorbance spectra of the growth gold surface in 100 µL MQ water were obtained at 400-800 nm wavelength range.

3.4.2.1. Ascorbic acid Concentration Optimization

To compare the ascorbic acid with NH_2OH, it was prepared with same dilution from stock and at same concentration. 0,05 M stock ascorbic acid solution was prepared first by dissolving 0,0088 g ascorbic acid with 1 ml MQ into an 1.5 ml eppendorf. Then, 0,025 M ascorbic acid solution was also prepared from 0,05 M reducing agent solution with diluted MQ into an different 1.5 ml eppendorf as 1 ml as total volume. Finally, 2 and 6 mM ascorbic solution were prepared from 0,025 M ascorbic solution.

20 µL of 5 mM gold solution and 80 µL of 2 and 6 mM ascorbic solution were added onto three solid gold surface. Firstly, the seeded gold surface spectra at 400-800 nm were taken into 100 µL MQ water to see gold growing effect at max wavelength shift. Growing process were performed depending on time as three parallel.

3.5. Refractive Index Sensitivity Measurements for Gold Surfaces

The measurements were carried out with sucrose, ethanol and BSA medium instead of MQ water. The different solid-state growth gold surfaces and seeded gold surfaces were used for these medium. The absorbance spectra of the immobilized Au into the three different medium respectively were measured as well.

3.5.1. Sensitivity Measurement for Gold Surface with Sucrose-Water

Sucrose solutions were prepared as 0-50% w/v with MQ at 10% increment in 20 ml vials respectively. 1, 2, 3, 4 and 5 g of sucrose were respectively dissolved in 10 ml MQ water by shaking with hand. The analysis was made as soon as they were prepared. Firstly, the spectra for non-growth and growth Au on solid surface were taken into MQ water. Then, by starting lowest concentration, the spectra were obtained into 100 μL sucrose solution at which concentration was taken in. The wells were washed with MQ water twice while passing to different concentrations.

3.5.2. Sensitivity Measurement for Gold Surface with Ethanol -Water

Ethanol solutions were prepared as volume range of 0-100% v/v with MQ at 10% increment in 2 ml eppendorfs respectively and rapidly due to ethanol volatility. The analysis was made as soon as they were prepared. Firstly, the spectra for non-growth and growth Au on solid surface were taken into MQ water. Then, by starting lowest concentration, the spectra were obtained into 100 μL ethanol solution at which concentration was taken in. The wells were washed with MQ water twice while passing to different concentrations.

Table 3.3. Preparation of Ethanol-water solutions

% concentration	Volume of Ethanol (μL)	Volume of Water (μL)
0	-	1500
10	150	1350
20	300	1200
30	450	1050
40	600	900
50	750	750
60	900	600
70	1050	450
80	1200	300
90	1350	150
100	1500	-

3.5.3. Sensitivity Measurement for Gold Surface with BSA

BSA solutions were prepared as 10 mg ml^{-1} and 20 mg ml^{-1} with PBS in 2 ml eppendorfs respectively. Firstly, the spectra for non-growth and growth Au on solid surface were taken into PBS. Then, by starting lowest concentration, the spectra were taken into 100 μL BSA solution at which concentration was taken in. The wells were washed with PBS twice while passing to other concentration.

3.6. Characterization Analysis of Gold in Solution and Growth Gold on Solid Support

3.6.1. Size Analysis of Synthesized Colloidal Gold Nanoparticles via Zeta-sizer

Gold nanoparticles size analysis was made 24 hour after synthesis. 1,5 ml of synthesized gold solution was diluted with 1,5 ml of MilliQ water in a 20 ml vial. Then, 2 ml of the diluted gold solution was poured into disposable polystyrene cuvette and sonicated about 3 min by ultrasonic bath. The particles' size in the solution was measured using zeta-sizer in triplicates. Before the start of measurement, the specific conditions were adjusted: refraction index of gold: 0,183; absorption of gold: 6,810; solvent: water and temperature: 25 °C; equilibrium time: 30 sec. The size analysis was also made for the synthesized colloidal gold solution without dilution at same condition.

3.6.2. Spectrophotometric Analysis of Seeded and Growth Gold Surface

The analysis was performed fast mode at 400-800 nm with 1 nm step size and without temperature controlling but the instrument temperature was in range 20-25 °C.

The absorbance spectra of the synthesized GNPs solution and diluted 1:1 synthesized GNPs solution were obtained 24 hour after synthesis. The measurement was operated after as soon as immobilization or growth Au was made. For refractive index sensitivity measurement with sucrose, ethanol and BSA, the spectra were taken into their solvent and the wells were washed with 300 µL MQ water.

3.6.3. Morphological Characterization of Seeded and Growth Gold Solid Surface

3.6.3.1. Scanning Electron Microscopy (SEM) Analysis

PMMA sheet were cut as 10 mm x 10 mm by laser cutter after drawing Corel-draw software. The slides were coated with aluminum foil as far as possible smoothing and were used for SEM characterization due to better conductivity. The slides were cleaned with ethanol and followed with MQ water and then placed the slides into a petri dish separately. After that, the same procedure for Au immobilization and Au growth on solid support was applied. However PLL solution was prepared into MQ water instead of PBS to eliminate the observing salts at SEM images. After 50 µL of the gold particles immobilization onto 100 µL of 0,05 mg/ml PLL, the growing Au on the slides was made with adding 20 µL of 5 mM $HAuCl_4$ and 80 µL of 6 mM NH_2OH to each gold surface. Growing process were performed in two minutes from four to ten minutes. After discarded growth solution at specific time onto each gold surfaces, they were washed with 100 µL MQ water three times. SEM analysis was made few days after growing. The surfaces were dried one or two days before analysis with discarding MQ onto the slides and then covering top of petri dish with napkin to so as not to touch the surface. SEM images were taken at 3 and 1 µm scale bar with 50000 and 100000 magnitude respectively.

The analysis of SEM images were made by using ImageJ 1.50i program. For finding of particle size distribution for each image, after setting scale the diameter of

thirty particles was measured by trying to be as accurate as possible. Histogram of particle size distribution taken from thirty particles was created via Originpro 8 program. In addition, percent particle area against background was being calculated using ImageJ by taken ratio of particles area to background area. The area analysis was made also for other two 300*300 um selected areas from different place and then the average particle area of three was taken.

3.6.3.2. Atomic Force Microscopy (AFM) Analysis

Glass slides were cut as 10 mm x 10 mm by laser used as surface for AFM substrates. The slides was cleaned with ethanol and followed with MQ water. The same procedure for gold immobilization and gold seeded surfaces was applied. However, PLL solution was prepared into MQ water instead of PBS to eliminate the observing salts at AFM images and 1:5 diluted synthesized Au colloidal solution was utilized for the surface instead of 1:1 dilution. After 50 µL of the gold particles immobilization onto 100 µL of 0,05 mg/ml PLL, the growing Au on the slides was performed by adding 20 µL of 5 mM $HAuCl_4$ and 80 µL of 6 mM NH_2OH to each gold surface. Growing process were performed in each minute from one to three minutes. After discarded growth solution at specific time onto each gold surfaces, they were washed with 100 µL MQ water three times. AFM analysis was made few days after growing. AFM characterization was worked with 2 µm scan size and on tapping mode. The analysis of AFM images was done by using NanoScope analysis version 1.40 software.

3.6.4. Artificial Neural Network based Characterization of Seeded and Growth Gold Solid Support

After gold seeding onto solid gold surface, the absorbance spectra for surfaces were recorded with the samples of sucrose-water mixtures which prepared at 0-50% concentration. An Artificial Neural Network (ANN) formulation was constructed and the data obtained from spectra was introduced to program. The 80% of samples were used to train the program and the rest was used as test samples. For this analysis, *Neural Network Toolbox* at MATLAB was used and ANNs different numbers of hidden layers and different number of neurons in these hidden layers were run 100 times.

Performances of employed ANNs were compared by taking the mean absolute error values of the test data set. Principle Component Analysis was also used with ANNs. In all ANNs, the Scaled Conjugate Gradient Back-propagation Algorithm was chosen and the regularization parameter was taken as 0.7.

3.7. Detection of Bacteria

All materials were sterilized by autoclaving (at 121 °C for 15 minutes) and used as sterile. In order to remove the foreign bacteria present in the medium, the working medium was wiped with 70% ethanol.

3.7.1. Bacterial Stock Preparation

E. coli DH5-alpha and *E. coli* BL21(DE3) bacterial strains were used in experiment. First, 50% glycerin stock was prepared with 6.5 ml sterile water then 2 ml of 50% glycerin was added onto 2 ml of bacterial strains in LB Broth respectively. Finally, the strains were aliquoted into eppendorfs and then stored at -20 °C.

3.7.2. Bacterial Growth Monitoring

50 µL of bacterial stock solutions were taken into 1,5 ml eppendorfs and diluted to 1000 µL with LB broth medium. The bacterial suspensions were allowed to incubate overnight at 240 rpm, 37 °C. The optical density (intensity at a specific wavelength, OD) of *E. coli* DH5-alpha and *E. coli* BL21(DE3) bacteria at 600 nm was measured at specific time intervals by microplate spectrophotometry for 21 hours to examine bacterial growth.

3.7.3. Bacteria Immobilization on Gold Surface

Bacterial strains in LB Broth medium and in PBS were immobilized onto non-growth and growth gold surfaces. Initially, the gold surfaces' absorbance was measured at 400-800 nm range in PBS medium. Later, OD at 600 nm was monitored for the

overnight cultured growing bacteria. For the *E. coli* BL21(DE3) strain in LB Broth adsorption, 100 µL of the overnight cultured bacterial solution were added onto non-growth, 4, 10 and 12 min gold seeding surfaces. The absorbance at 600 nm was obtained at every 30 min until six hours for the each non-growth and growth gold surfaces respectively. At final step, the absorbance was measured in PBS medium after discarding bacteria and washing with PBS three times. For the both strains in PBS adsorption, the overnight cultured *E. coli* BL21(DE3) and *E. coli* DH5alpha in the LB medium was centrifuged at 4000 rpm and for 8 minutes to separate the bacteria from the medium. At the end of the centrifugation, the supernatant was discarded by pipetting, and the remaining bacteria on the bottom of the tube were washed with 1 ml of PBS and centrifuged again. 100 µL of bacterial solutions in PBS were added onto the non-growth surface and 4 min growth gold surface. The spectra of bacterial strains adsorption on gold surfaces in PBS medium were obtained at range of 400-800 nm after 90 min incubation time after discarding bacteria and washing with PBS three times.

The *E. coli* BL21(DE3) in PBS was also adsorbed onto gold surfaces for SEM analysis. The gold surfaces for SEM were prepared with the same procedure which was described above at section 3.6.3.1. Moreover, there was also a PLL surface in addition to non-growth, 4 min and 10 min growth gold surfaces to see the effect of cationic surface to bacteria binding. In addition, the bacterial suspension was prepared in sterile water instead of PBS. The suspension was added as 50 µl on the surfaces and after 30 min and 60 min incubation time respectively, the surfaces were washed with sterile water three times. Then, they was left to dry at +4 °C for one day with covering top of petri dish with napkin to so as not to touch the surface.

3.7.3. Bacteria into Commercial Goods Screening on Gold Surface

The two overnight cultured *E. coli* BL21(DE3) bacterial solutions were washed once with sterile water. The commercial milk and apple juice were injected onto a bacterium pellet respectively. After taken spectra of gold immobilized and 4 min gold seeding surfaces in sterile water, the bacteria containing milk and juice were adsorbed on the gold surfaces for 30 minutes. Subsequently, the spectra of adsorbed bacteria were obtained in sterile water at range of 400-800 nm after discarding bacteria and washing

with sterile water three times. The experiment was repeated three times and the different surfaces were used for both goods.

CHAPTER 4

RESULTS & DISCUSSIONS

4.1. Synthesis and Characterization of Gold Nanoparticles in Solution

The characterization of gold nanoparticles was done after synthesis is completed. The color change from light gray to wine-red was observed during time after citrate addition as shown in Figure 4.1 and it was observed that the reaction was complete after one day. The color of gold solution (yellow) turned to wine-red rapidly after addition of citrate solution demonstrating the higher reactivity that provides faster nucleation and growing.

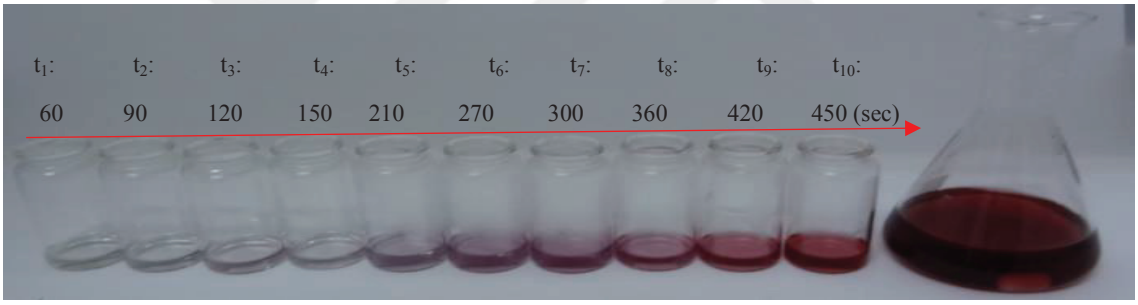

Figure 4.1. The color changes of colloidal gold solution during time. The light gray represents the gold solution after citrate addition to pale yellow gold solution and reddish color represents colloidal GNPs formation

4.1.1. Size Analysis

Size analysis of synthesized GNPs was done by using Malvern ZS Zeta-Sizer. Zeta-sizer gives an idea about average size of nanoparticles and also enables to track aggregation behavior. Figure 4.2a shows size distribution by intensity obtained from the synthesized colloidal gold solution. The average of GNPs corresponds to the intense peak from three replication is at 18,71 nm. The presence of aggregates was also obtained by a multimodal distribution which was at about 170 nm and 5000 nm with very low, 2%, intensity. The aggregate may be obtained from precipitated citrate.

Nevertheless, the aggregate concentration is relatively low when intensity based distribution is converted to a volume as demonstrated in figure 4.2b. The size distribution by volume confirms that the majority of the sample on the base of mass is composed of small particles that are around 13 nm. In addition, the monomodal distribution around 10,87 nm is seen at size distribution by number in figure 4.2c, which shows few aggregates in synthesized gold solution. Therefore, it can be said that, the vast majority of the available particles are very small in diameter small which makes it difficult to calculate the total aggregate concentration. In addition, polydispersity index (PDI), which is a measure of size distribution, shows if aggregation present. The PDI of the colloidal gold solution was obtained as 0,371 indicating almost monodisperse solution and has a narrow size distribution. Table 4.1 summarize the Zeta-sizer results of synthesized GNPs.

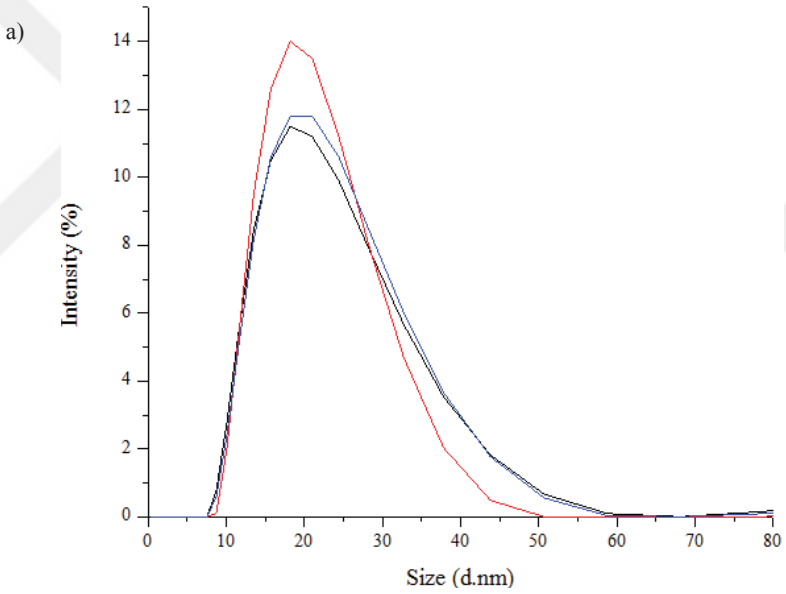

Figure 4.2. Size distribution of synthesized GNPs by a) intensity b) volume c) number

(cont. on next page)

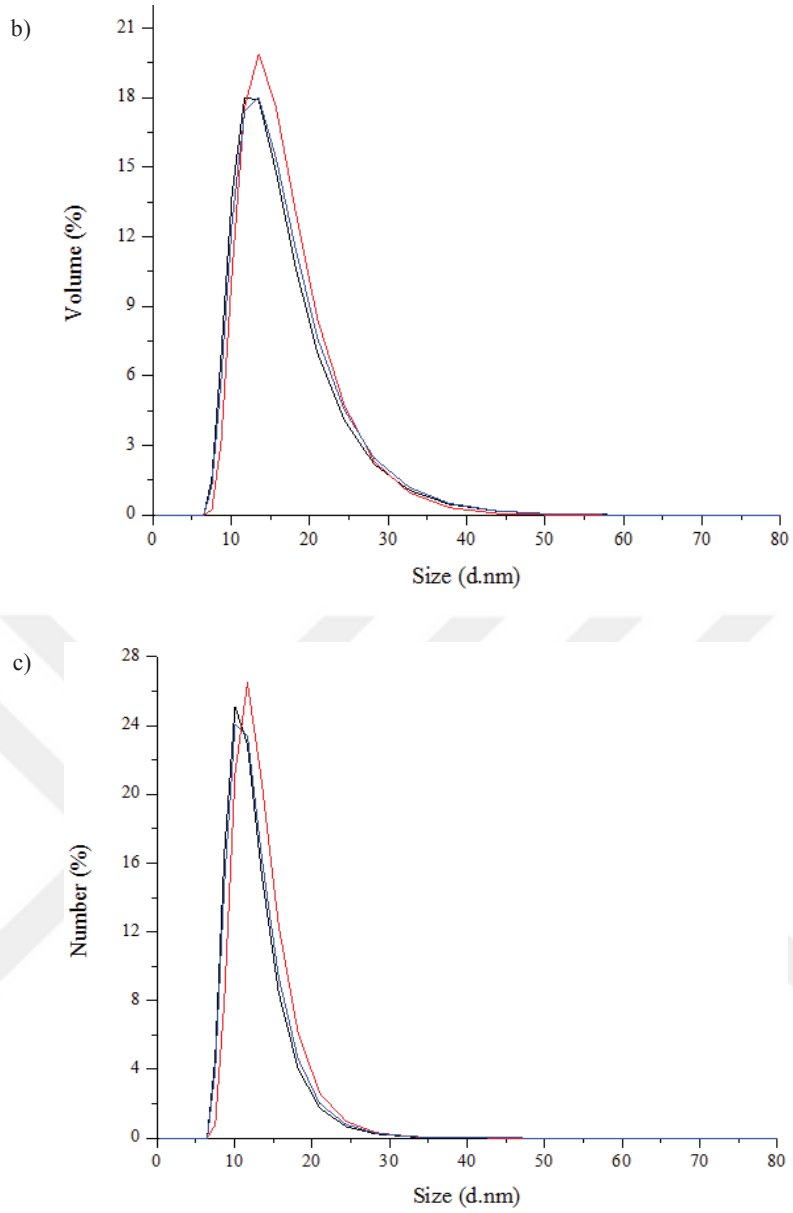

Figure 4.2. (cont.)

Table 4.1. Average size of GNPs in solution obtained from Zeta-sizer

	Intensity	Volume	Number
Average Size (nm)	18,71	12,88	10,87
PDI	0,371	0,371	0,371

4.1.2. Spectrophotometric Analysis in Solution

Spectrophotometric analysis can confirm the formation and stability of the nanoparticles, and colloidal GNPs exhibit a very specific color caused by Localized Surface Plasmon Resonance (LSPR) effect. The peak wavelength depends on diameter of gold nanoparticles; for gold nanospheres it is generally between 520-540 nm. The larger wavelengths are related to anisotropic gold nanoparticles or larger gold nanospheres.

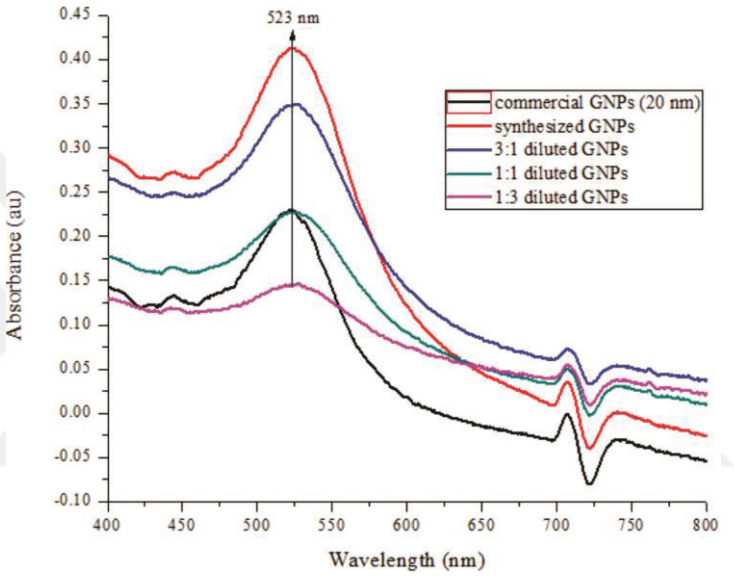

Figure 4.3. Absorption spectra of the synthesized gold nanoparticles. Comparison of varied dilutions (3:1, 1:1, 1:3) with commercial counterpart

As shown in figure 4.3, the absorbance spectra of the 20 nm commercial GNPs (753610, Aldrich) was compared with synthesized gold nanoparticles at varied dilutions. It shows that the absorbance intensity of 1:1 diluted GNP absorbance is similar to the commercial counterpart. Therefore, the synthesized GNPs solution was used after 1:1 dilution for further experiments. In addition, the graph demonstrates that the concentration change only affects the intensity of the peak but not maximum wavelength. Figure 4.4 shows the synthesized and 1:1 diluted colloidal GNPs in MQ water. The maximum wavelength is 522 nm for both concentrated (red-wine color) and 1:1 diluted GNPs. Absorption maximum at 522 nm confirms the size of synthesized gold nanoparticles is around 20 nm without anisotropic gold nanoparticles. However,

we can see the peak after 700 nm for synthesized GNPs in distilled (DI) water rather than in MQ. Therefore, there is no single peak and it may be coming from impurities because of water quality. The gold ions are reacting with impurities or metals in DI water, so they can form anisotropic gold or agglomeration.

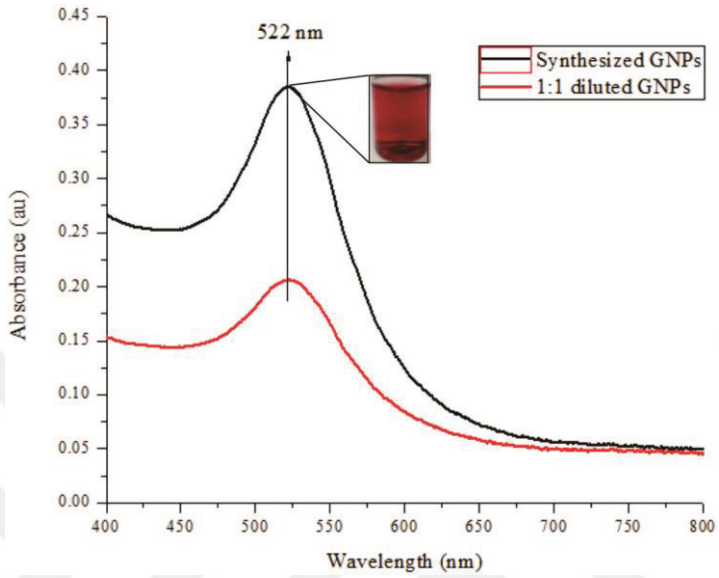

Figure 4.4. Full absorption spectra of the synthesized gold nanoparticles in MQ

4.2. Spectrophotometric Analysis on Solid Support

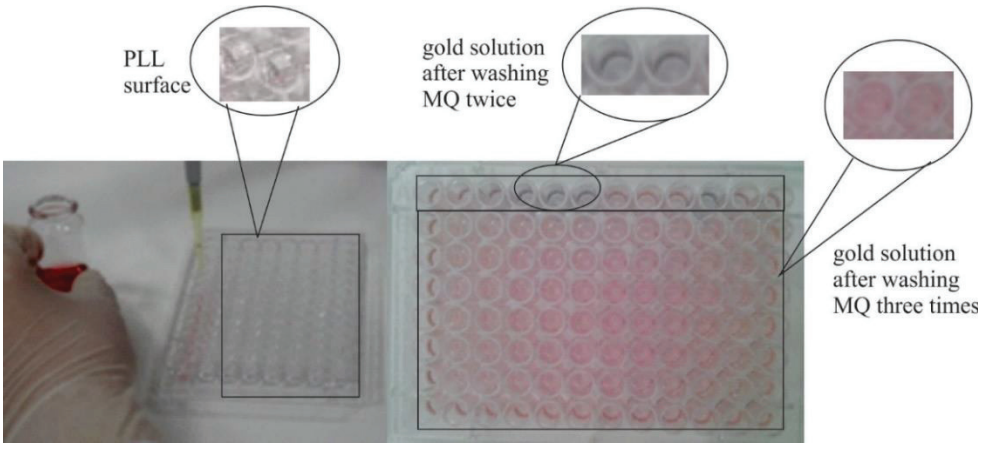

Figure 4.5. GNP immobilization onto the PLL modified solid support

The synthesized GNPs in aqueous solution have net negative charge based-on citrate capping, so they react with positive amine group at PLL. Therefore, GNPs were

immobilized onto solid support by utilizing electrostatic interactions. After immobilization of GNPs the color of the solid surface turns from colorless to pink as shown in Figure 4.5. Immobilized GNPs were used as a seed particle on the surface for further growth and characterization steps.

4.2.1. Concentration Optimization for Immobilization on Solid-Support

Synthesized GNPs were diluted with MQ water, and the effect of GNP concentration on immobilization process was examined. As shown in Figure 4.6, increasing GNP concentration on the solid surface causes the red shift in absorption spectrum. Absorption spectrum obtained from the surfaces of the 96 well-plate confirms the successful immobilization of GNPs on solid support. The plasmon peak (absorbance maximum) is 534 nm for 1:1 diluted and then immobilized GNPs, while it is 540 nm for immobilized GNPs without dilution. More concentrated GNP solution may cause agglomeration or accumulation of GNPs on the surface due to higher surface coverage ratio.

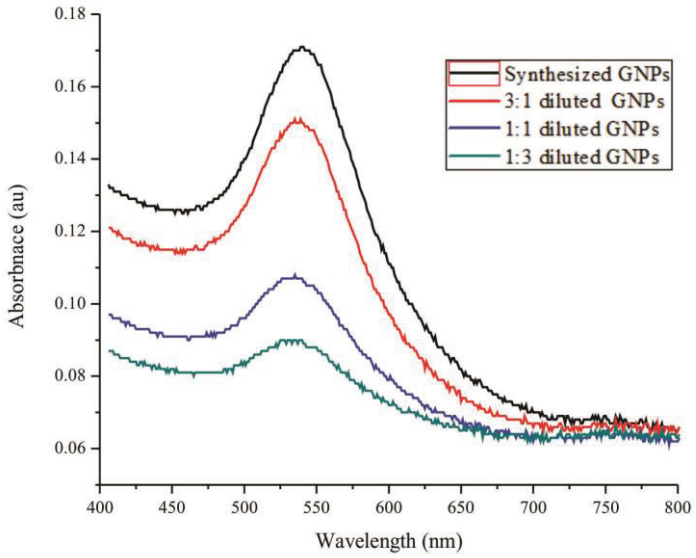

Figure 4.6. Absorption spectra of the immobilized GNPs at different concentration

When PBS is used instead of MQ or DI water it was seen that more than half of the GNPs were agglomerated on the solid surface, so immobilized gold surfaces were not homogeneous. Therefore, prior to GNP immobilization surface was rinsed with MQ

three times since insufficient washing can cause agglomeration of gold, which has violet color if the salt residue or impurity is present as shown in Figure 4.5. To prevent the agglomeration, which is caused by the ionic interaction between residual PBS and GNPs, GNP immobilized surfaces was washed with MQ three times at each step during all experimental procedure.

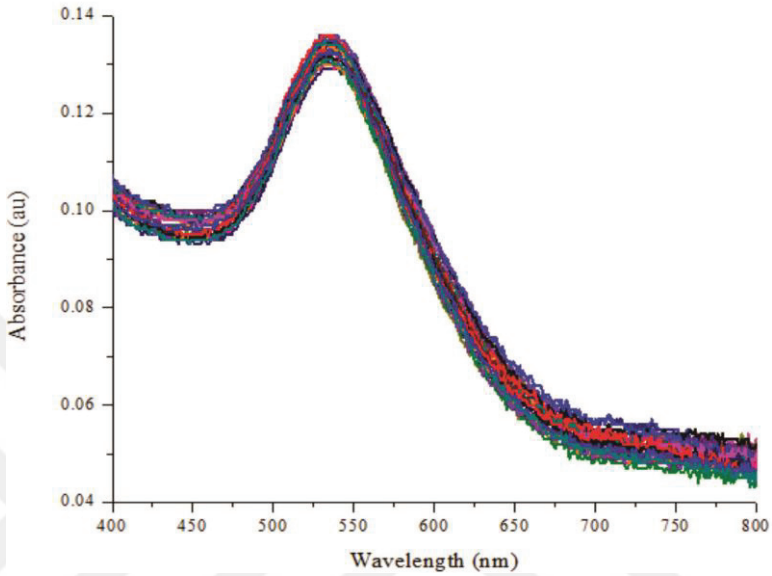

Figure 4.7. Absorption spectra of the immobilized GNPs on solid support for 32 wells

As shown in Figure 4.7, homogeneous immobilization of citrate capped GNPs was achieved at 534±1 nm due to electrostatic interaction of GNPs with PLL functionalized surface. There is a 12nm red shift compared to colloidal GNP solution indicating immobilization of GNPs on solid support. The immobilization of GNPs on a solid support differs from solution. Immobilization onto solid support changes both the intensity and position of plasmon peak, and it also affects the optical properties that can be further confirmed by naked-eye.

4.3. Characterization of Gold Nanoparticle Growth on Solid Support

Growth of GNPs was done on solid support by utilizing both strong reducing agent (hydroxylamine hydrochloride) and mild reducing agent (L-ascorbic acid) separately at room temperature. The growth was made with adding 20 µL gold solution onto immobilized GNP surface and then immediately adding 80 µL reducing agent onto

same surface, without dipping gold sample into high volume of growth solution like at literature.[48, 76-78] The experimental schematic of GNP growth on solid surface was illustrated in Figure 4.8. The size of immobilized seed particles is increased with reducing Au^{3+} ions on surface directly, so that the gap between the particles is decreased. As a result the hot spot providing higher sensitivity with plasmon coupling effects was achieved compared to solution-based systems.

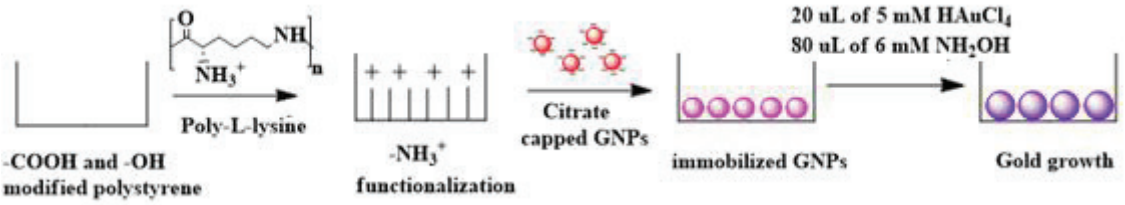

Figure 4.8. Schematic of the GNP growth on solid-support

4.3.1. Optical Analysis

4.3.1.1. Gold Growth with Strong Reducing Agent

The reduction of 5 mM Au ions with 6 mM NH_2OH on GNP immobilized solid surface was shown in Figure 4.9, 4.10 and 4.11. Each figure represents different growth time frames for varying seed GNPs. The different size of seed GNP depends on solution based synthesis properties. Each spectrum was taken from different GNP immobilized surfaces in MQ water at room temperature. As represented in the graph, the starting wavelength is directly affected by the size of immobilized GNPs on solid surface. When the smallest initial plasmon peak is observed for the immobilized GNP, the faster growing is induced. Thus, during the same growth time under the same experimental conditions the growth of smallest seed GNPs is faster than the larger ones. A shift at LSPR peak gives information about particle size and structure. When correlated with the LSPR peak wavelength and the size of the GNP[8, 27, 79], about 40 nm GNP seed can grow up to above 100 nm (Fig. 4.9), however about 50 nm GNP seed can grow up to 100 nm (Fig. 4.10-4.11) during same time frame, indicating that size of the seed particle is the most effective parameter on growth kinetic and final size of the particles on the surface.

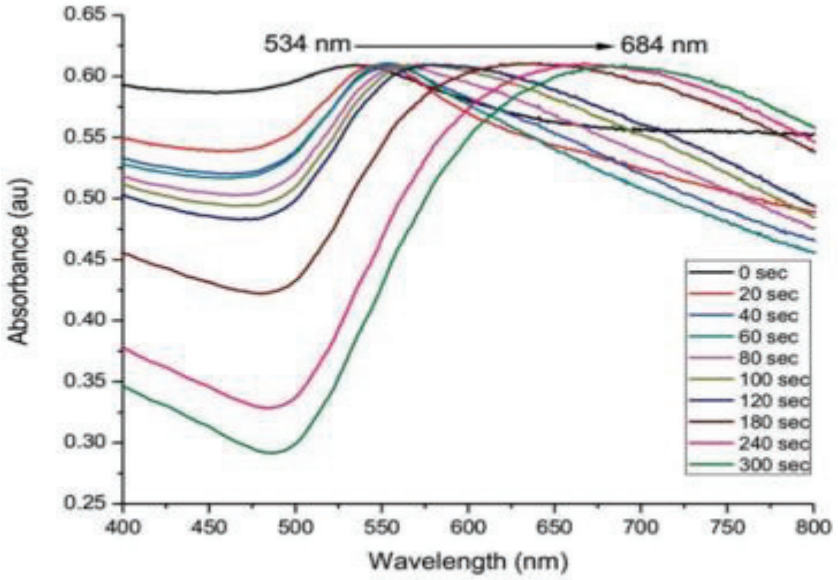

Figure 4.9. Normalized surface plasmon absorption spectrum of the solid-state growth of GNPs with 534 nm max starting wavelength

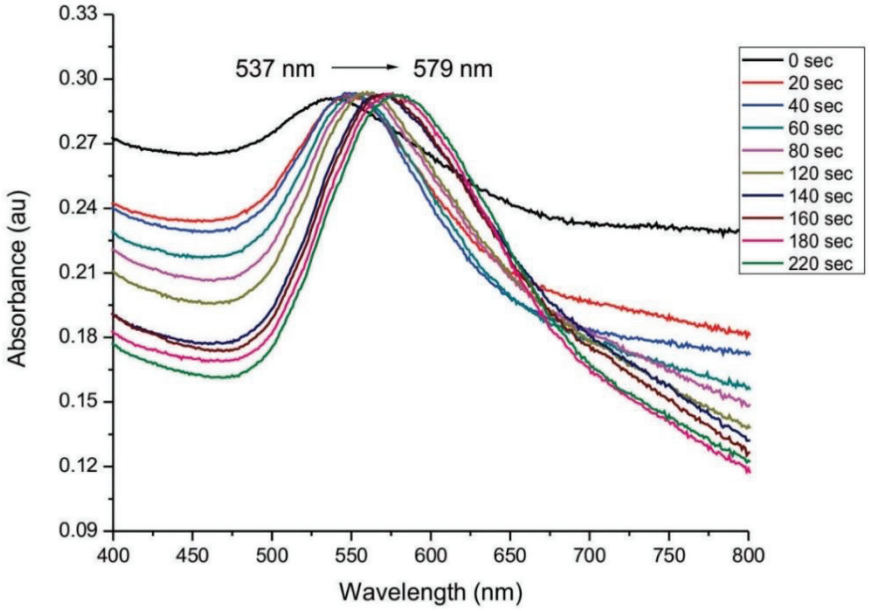

Figure 4.10. Normalized surface plasmon absorption spectrum of the solid-state growth of GNPs with 537 nm max starting wavelength

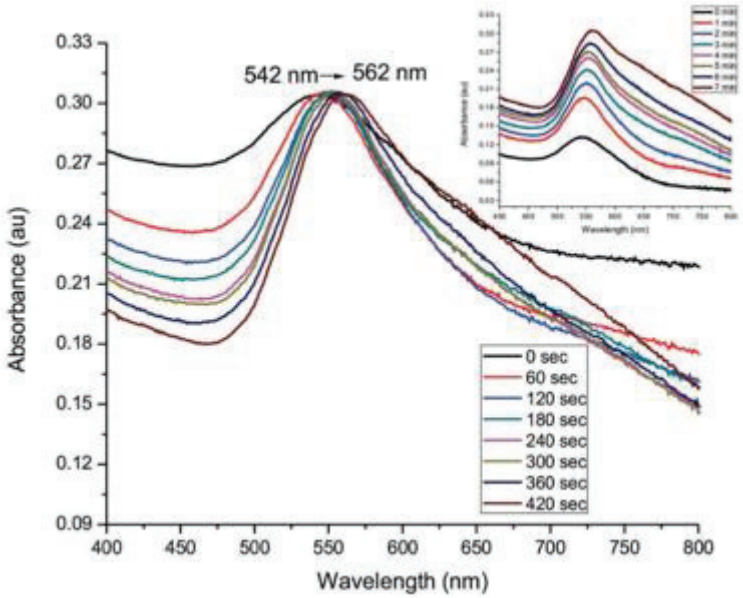

Figure 4.11. Normalized surface plasmon absorption spectrum of the solid-state growth of GNPs with 542 nm max starting wavelength

4.3.1.1.1. Concentration Dependency on Gold Growth Kinetics

Gold growing kinetics was examined through screening of optical density (OD) at 580, 590, 595, 600 and 605 nm. Concentration dependency was investigated by using different concentrations of NH_2OH with 5 mM $HAuCl_4$, and the results are shown in Figure 4.12, 4.13 and 4.14. To observe the concentration dependency 2, 4, 5, 6, 8 and 10 mM NH2OH solutions were applied to the GNP immobilized solid surface in the presence of $HAuCl_4$. Growth kinetics was monitored continuously in 100 µL growing solution without discarding and washing, so growth of GNPs on solid support was observed directly from growing surface. 580-605 wavelength range was used since this region is the most sensitive area to the RI changes around max plasmon peak. The figures show that depending on the reducing agent concentration absorbance reaches to max value at different time intervals. While 6, 8 and 10 mM NH_2OH samples reaches to the saturation absorbance in 4 to 6 mins 2, 4 and 5mM NH_2OH samples reaches to saturation in more than 8 mins. For usage of equal or lower concentration of $HAuCl_4$, the time is extended because the power of reducing gold ions was decreasing as decreasing the reducing agent's concentration, so that the induction time was lower. It is observed that growing with 6 mM NH_2OH, the reducing agent and growing reaction is more controlled so this parameters were fixed following characterizations parts.

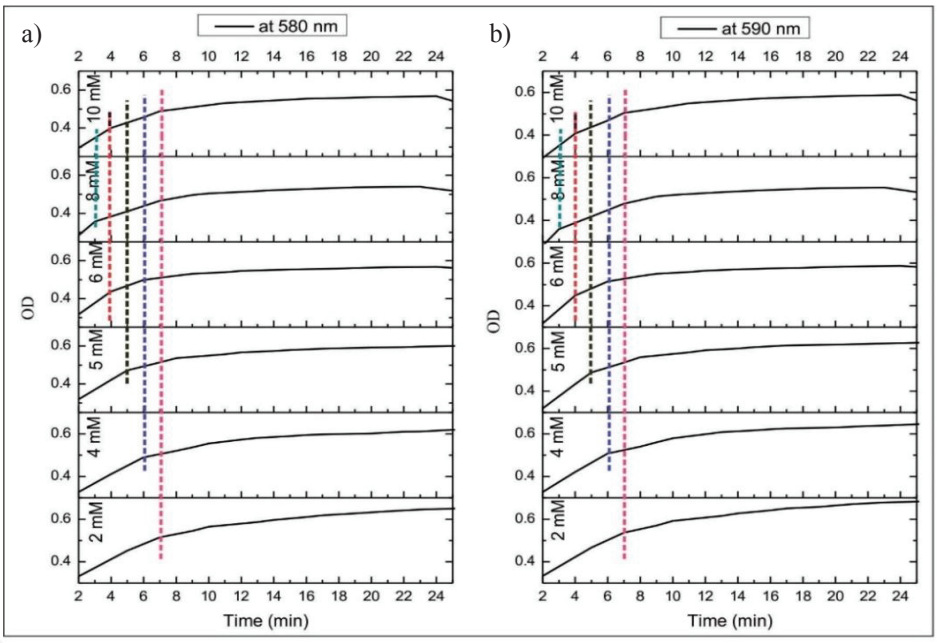

Figure 4.12. Screening of the gold growth on solid-state at a) 580 nm b) 590 nm with varied NH_2OH concentrations; 2, 4, 6, 8 and 10 mM NH_2OH

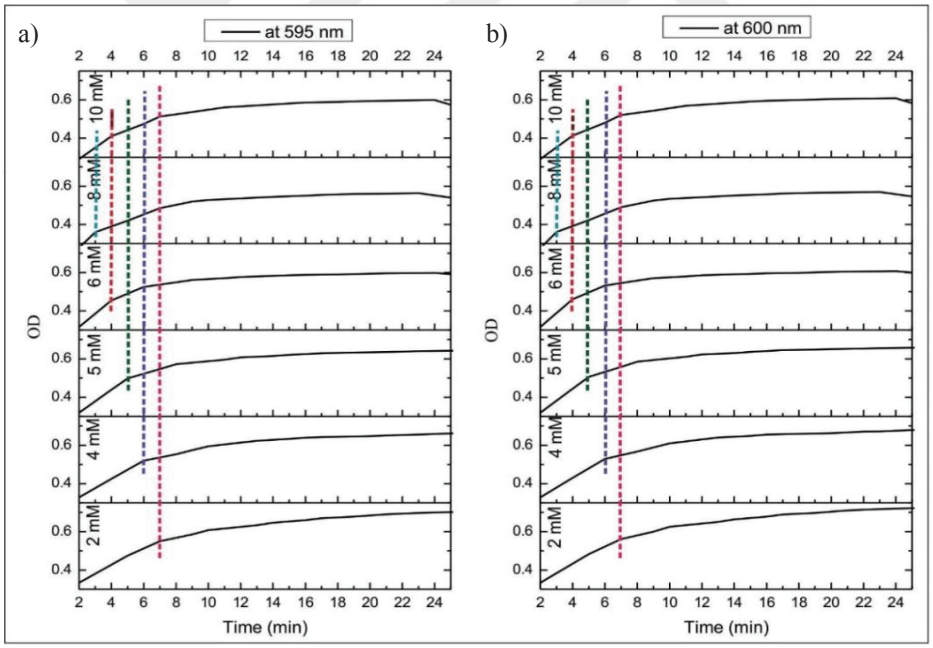

Figure 4.13. Screening of the gold growth on solid-state at a) 595 nm b) 600 nm with varied NH_2OH concentrations; 2, 4, 6, 8 and 10 mM NH_2OH

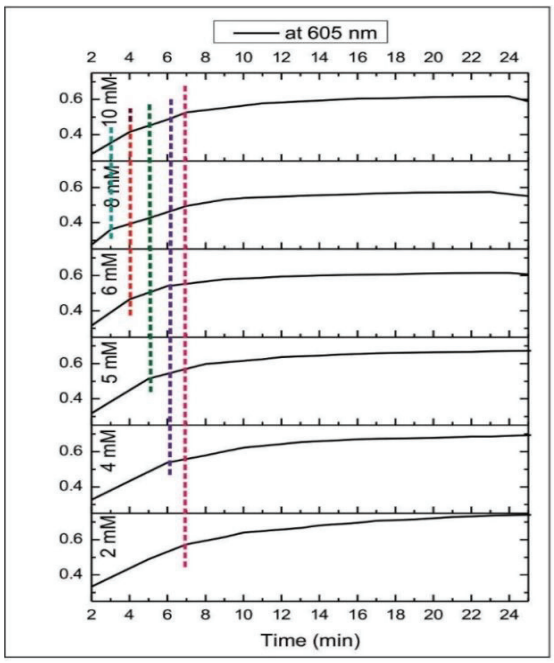

Figure 4.14. Screening of the gold growth on solid-state at 605 nm with varied NH_2OH concentrations; 2, 4, 6, 8 and 10 mM NH_2OH

4.3.1.1.2. Time Dependency on Gold Growth

Full absorbance spectrum was also collected in static mode from gold growing surfaces as illustrated in Figure 4.15, 4.16 and 4.17. The growing GNPs cause the LSPR shift due to plasmonic coupling. However, it was observed that after certain time the gold growth is terminated even if the time increased. This shows the growing isotropic GNPs are limited. Depending on the reducing agent concentration, the plasmonic band can be broader, and takes longer to reach certain size of nanoparticles. The changes at plasmon band can be obtained from two pathways; either a new particle nucleation or nanoparticle growth. However, only maximum surface plasmon shifts were obtained at full spectra depending on residence time of gold growth solution on the gold surface and no other plasmon bands were obtained. Thus, it can be said that the growing of seed GNPs immobilized on the surface is more favored.

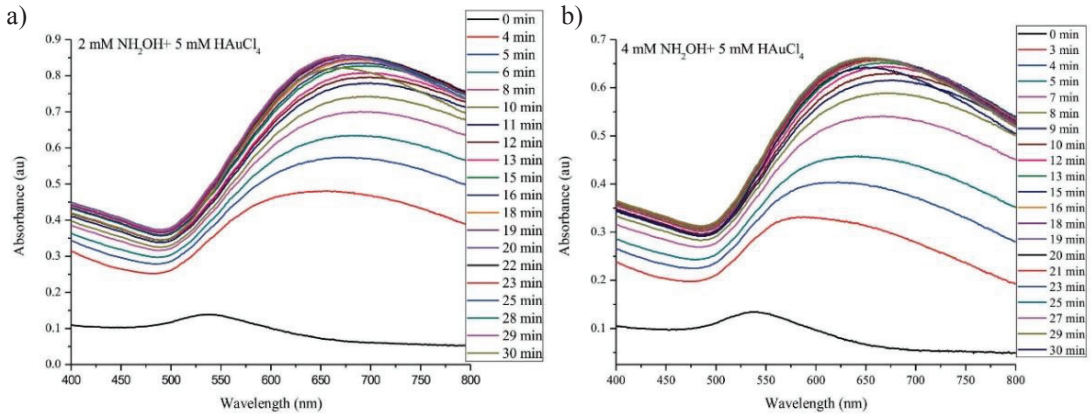

Figure 4.15. Effect of time dependency on absorbance spectrum of the gold growth on solid-state a) 2 mM b) 4 mM NH_2OH with 5 mM $HAuCl_4$

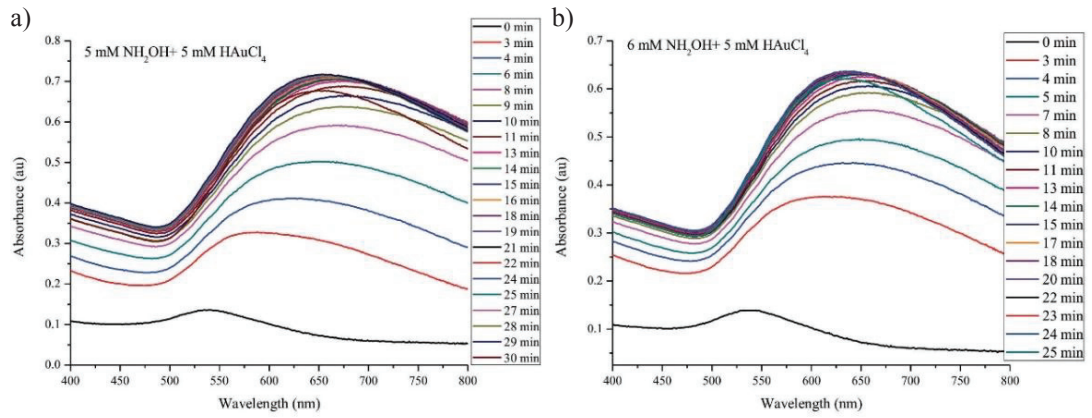

Figure 4.16. Effect of time dependency on absorbance spectrum of the gold growth on solid-state a) 5 mM b) 6 mM NH_2OH with 5 mM $HAuCl_4$

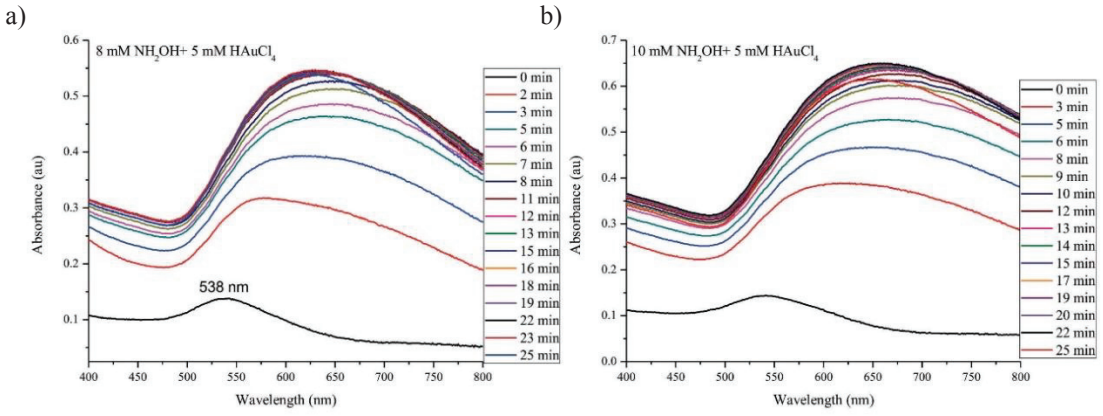

Figure 4.17. Effect of time dependency on absorbance spectrum of the gold growth on solid-state a) 8 mM b) 10 mM NH_2OH with 5 mM $HAuCl_4$

4.3.1.2. Gold Growth with Mild Reducing Agent

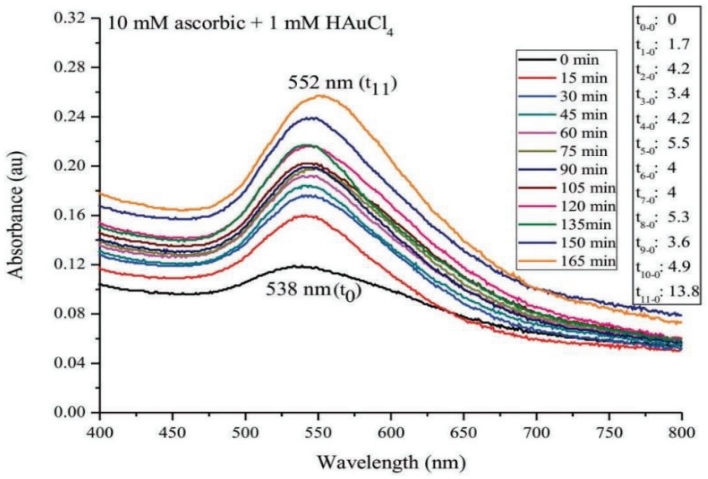

Figure 4.18. Absorption spectra of the solid-state GNPs growth with 10 mM L-ascorbic acid

A mild reducing agent, L-ascorbic acid, is utilized to observe the effect of reducing agent on gold growth conditions. Ascorbic acid is a milder reducing agent and weaker than hydroxylamine hydrochloride so it is expected it takes longer to complete reaction. Based on the literature, the concentrations of ascorbic acid and gold ions were adjusted. Ascorbic acid showed a low growth rate and non-stable growth. The Figure 4.18 show the change of max plasmon peak based-on time increment, which reaches up to 550 nm. During 165 min growing, there is only about 14 nm shift from plasmon peak corresponds to approximately 80 nm GNPs.

4.3.1.2.1. Concentration Optimization of Weak Reducing Agent

To optimize the concentration of weak reducing agent in kinetic mode, absorption spectrum was obtained from the surface in 100 µL growing solution without discarding and washing. As illustrated in Figure 4.19 spectrum is narrow but almost no growing is seen for lowest concentration of ascorbic acid. However, Figure 4.20 demonstrates that gold growth on solid surface can be achieved with 6 mM ascorbic acid and 5 mM $HAuCl_4$, but still around max at 550 nm. Therefore, it can be concluded

that for mild reducing agent like ascorbic acid, the concentration should be higher than gold precursor's concentration however still longer reaction time is required.

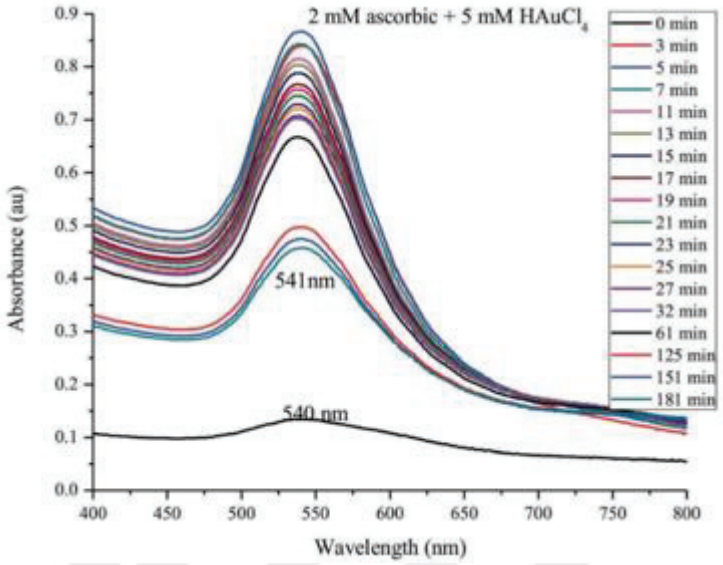

Figure 4.19. Time and concentration dependency on the solid-state gold growth with 2 mM ascorbic acid and 5 mM $HAuCl_4$

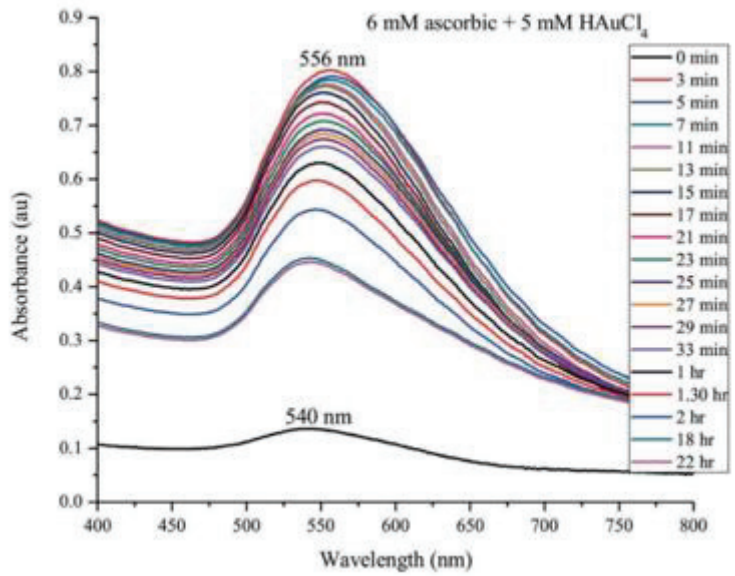

Figure 4.20. Time and concentration dependency on the solid-state gold growth with 6 mM ascorbic acid and 5 mM $HAuCl_4$

4.3.1.3. Analysis of Refractive Index Sensitivity

GNPs show specific LSPR behavior based-on their size and structure differences. Refractive index (RI) changes on the surface can be easily determined by LSPR since binding of analyte or ligand cause dielectric change in microenvironment. The sensitivity of developed plasmonic platform against RI changes was examined by using varied concentrations of sucrose, ethanol and BSA solutions. It was expected that depending on the RI change, which corresponds to concentration change, plasmon peak would shift so the analyte concentration can be analyzed. However solution-based LSPR systems have limited sensing capability due to low limit of detection. For detection of very low analyte concentration, the surface sensitivity should be increased. Thus, in this study a solid-state experimental plasmonic platform has been developed to increase the sensitivity and utilized for biosensing applications.

4.3.1.3.1. Sucrose Analysis

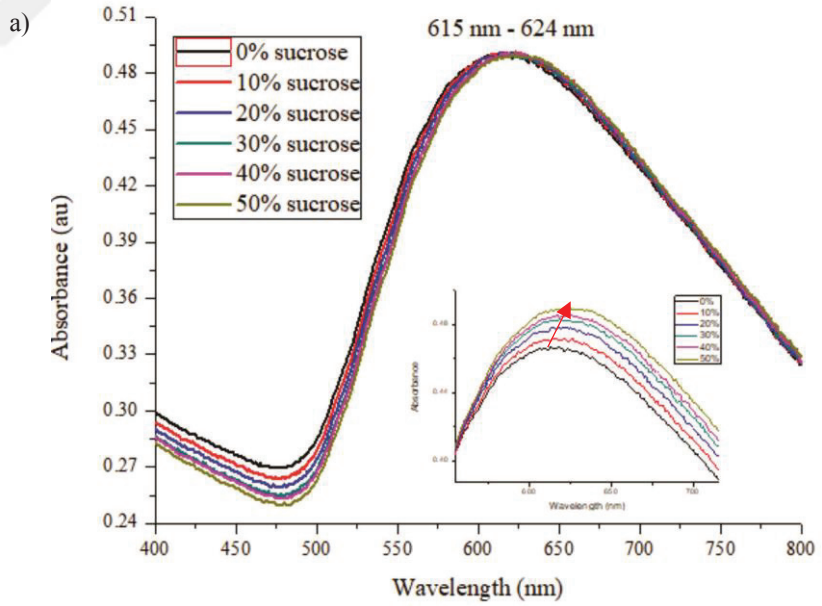

Figure 4.21. a) Normalized spectra of plasmonic platform in sucrose solutions (0-50 %), b) Correlation of LSPR maximum vs RI of the sucrose solutions

(cont. on next page)

b)

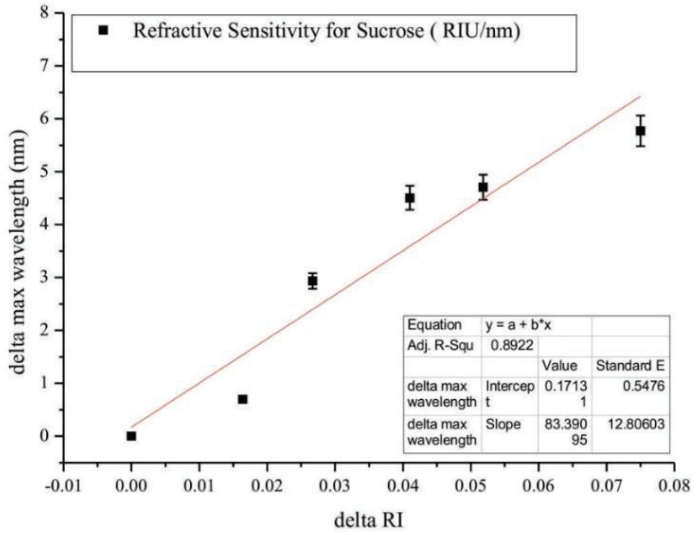

Figure 4.21. (cont.)

The RI sensitivity measurements were done by using gold growth platform with 7 min growing time. Sucrose solutions at a concentration range of 0-50% correspond to RI variation form 1,3315 to 1,4065. Figure 4.21 demonstrates the plasmonic platform differentiates the RI changes and red shift in LSPR peak is obtained due to the increasing dielectric constant of the medium.

4.3.1.3.2. Ethanol Analysis

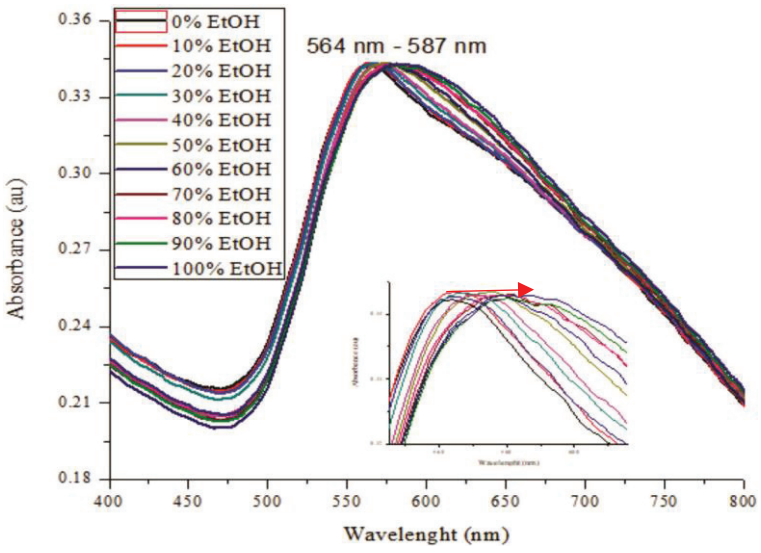

Figure 4.22. Normalized spectra of plasmonic platform in ethanol solutions (0-100 %)

The RI sensitivity measurements were done by using gold growth platform with 9 min growing time. Ethanol solutions at a concentration range 0-100% corresponds to RI variation from 1,3315 to 1,3665 (100% ethanol RI: 1,3635). Fig. 4.22 demonstrates the plasmonic platform differentiates the RI changes and shows the red shift in LSPR peak.

4.3.1.3.3. BSA Analysis

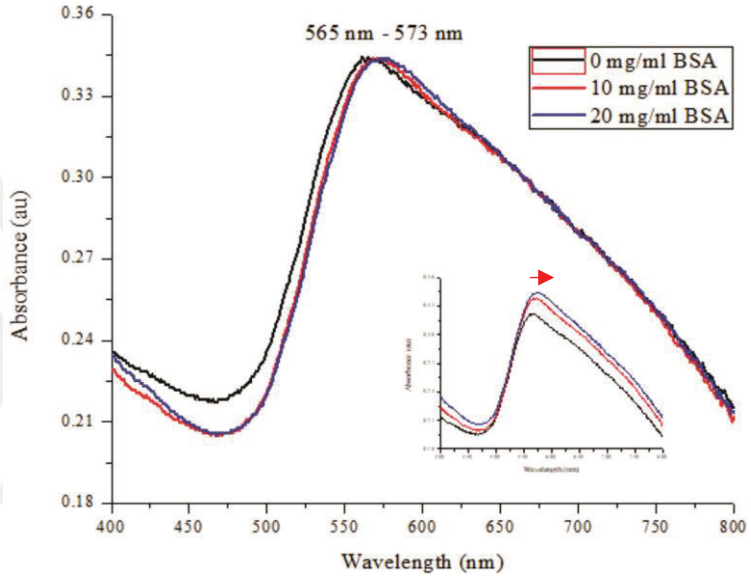

Figure 4.23. Normalized spectra of plasmonic platform in BSA solutions (0-20 mg /ml)

The RI sensitivity measurements were done by using plasmonic platform with a 9 min growing time. BSA solutions ranging from 10 to 20 mg ml^{-1} corresponds to RI variety from 1,333 to 1,3373. Fig. 4.23 demonstrates that the plasmonic platform differentiates the small RI changes, which is confirmed by 7 nm red shift in LSPR peak.

4.3.1.4. Artificial Neural Network (ANN)

After gold growing from 4 min to 13 minutes, the spectra at 300-800 nm range were plotted for gold surfaces into sucrose-water mixtures at 0-50%. For each concentration of sucrose the experiment was replicated 141 times. Artificial neural network (ANN) was constructed to guess the sucrose concentration and 80% of samples were used for training the program and the rest was used as test samples.

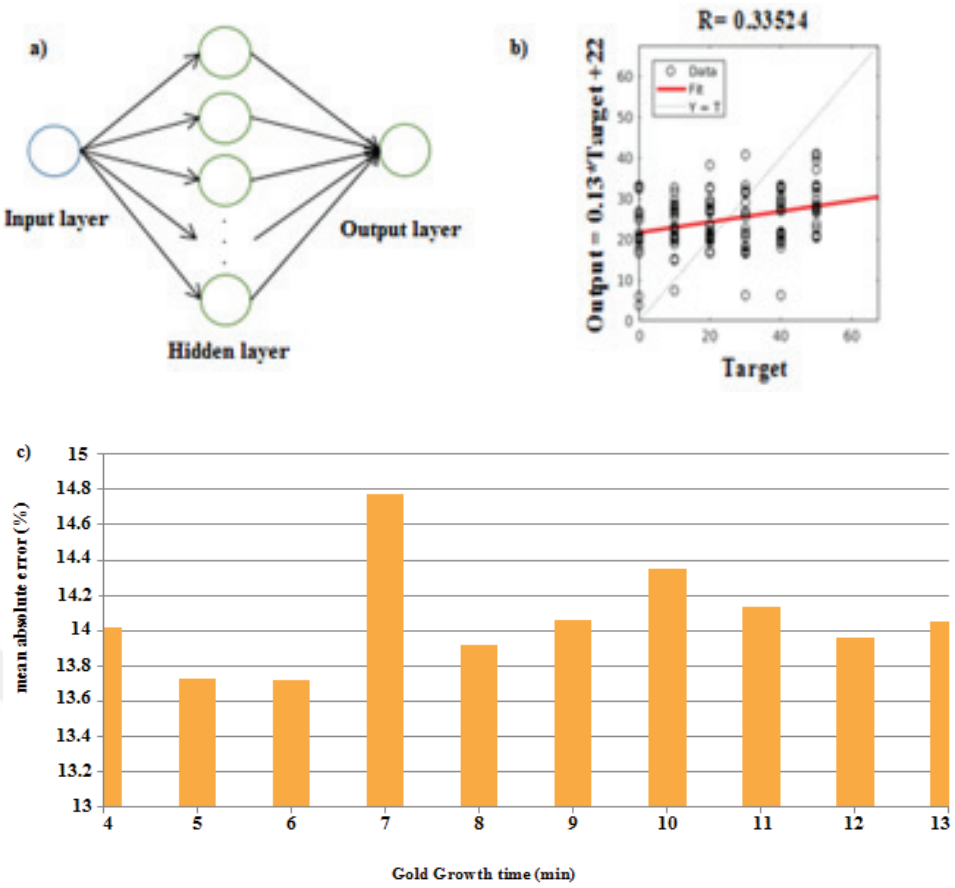

Figure 4.24. a) Formation of an ANN for plasmon resonance peak wavelength as the input layer, and one unit output layer b) results from ANN construction with LSPR peaks for 6-min data c) The mean absolute error for each min

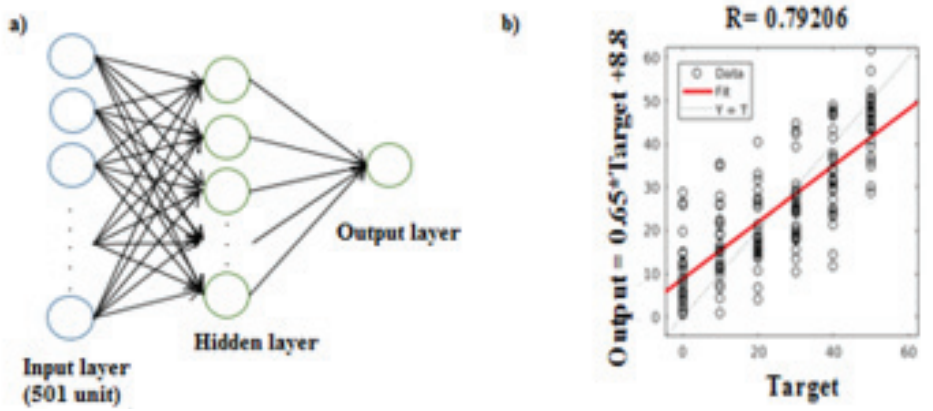

Figure 4.25. a) Formation of an ANN of 501 unit input layer, and one unit output layer b) results from ANN construction with all spectrum data for 6-min data

The wavelength where maximum plasmon peak occurs was used to discuss the refractive index sensitivity for our system and Fig. 4.24a shows the representative of construction of an ANN for plasmon resonance peak. However, Figure 4.24b shows the very high error which tells very weak correlation between output produced by ANN and actual sucrose concentration so the estimation of unknown sucrose concentration is nearly impossible. In addition, the mean absolute error was calculated for each min when spectrum max peak wavelength values are used and the results were shown in Figure 4.24c. The sucrose concentration can be estimated with about 14 percent mean error. Then, we tried to construct the ANN with each 501 wavelengths instead of peak maximum with one output as shown in Figure 4.25a. This formulation gave better results with strong relation between output produced by ANN and actual sucrose concentration as seen in Figure 4.25b.

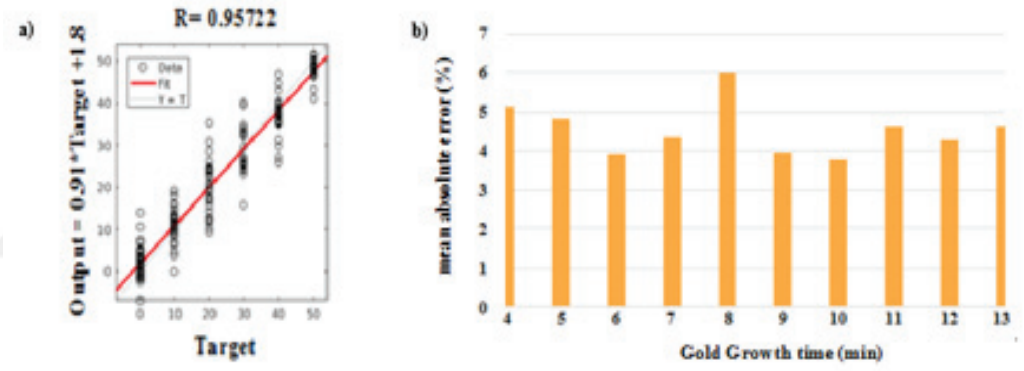

Figure 4.26. a) Results from ANN construction with all spectrum data after applying PCA for 6-min data; b) The mean absolute error for each min

The results were even improved by applying PCA to the data before giving them to ANN as shown Figure 4.26. Here, first 10 principal components were selected which encompasses 99.8% of the variance in the original data. Very strong correlation between producing output and actual sucrose concentration was achieved with 0.96 R value (Figure 4.26a). Moreover, the mean error to estimate the unknown sucrose concentration was also reduced up to about 4 percent (Figure 4.26b). Therefore, this technique can be alternative to get more accurate results in a short time by analyzing all data in spectrum instead of looking only one peak point in spectrum.

4.3.2. Morphologic Characterization of Gold Growth

4.3.2.1. SEM Analysis

The SEM image in Figure 4.27a shows successful and homogeneous coverage of immobilized GNP seeding on alumina surface and in Figure 4.27b-e gold growth on solid surface during 4, 6, 8 and 10 mins. Size of the growing GNPs was analyzed directly from SEM images by using ImageJ software[13]. The histogram confirms the increasing size of GNPs with the increased growth time on the solid surface. Without growing the size of the immobilized seed GNPs were around 14 nm, after gold growth size of the GNPs on the solid support reached to 17.5, 22.5, 32.5 and 40 nm for 4, 6, 8 and 10 mins respectively. The size distribution for immobilized GNPs was between 12 and 16 nm (Fig. 4.27a), which is lower than the synthesized size of GNPs in solution. For SEM analysis, the sample was used after blow-drying so the smaller size can be caused by dielectric environment change on the surface compared to the optical characterization results.

a)

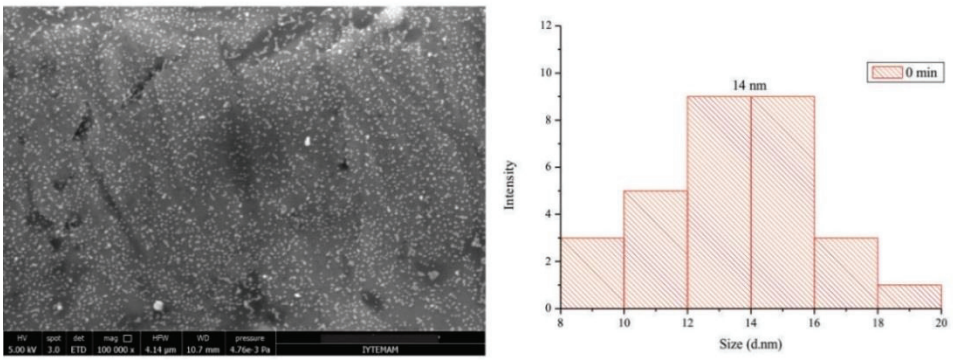

b)

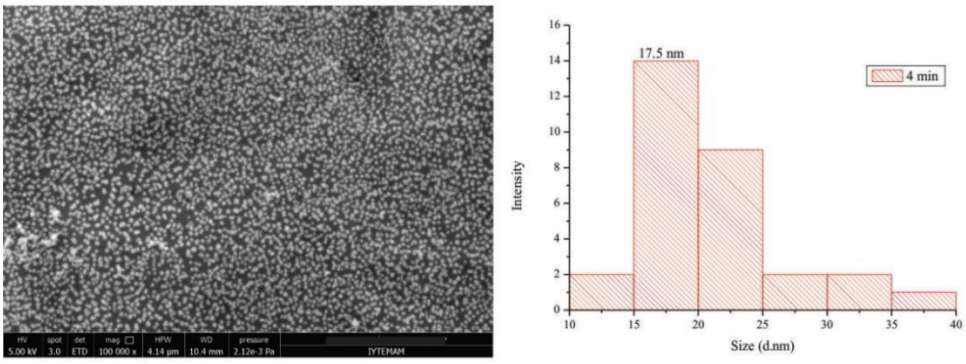

Figure 4.27. SEM images and corresponding size analysis histograms for a) immobilized GNPs on solid support (0 min) b-e) gold growth surfaces on solid support at 4, 6, 8 and 10 min (scale bar : 1 μm)

(cont. on next page)

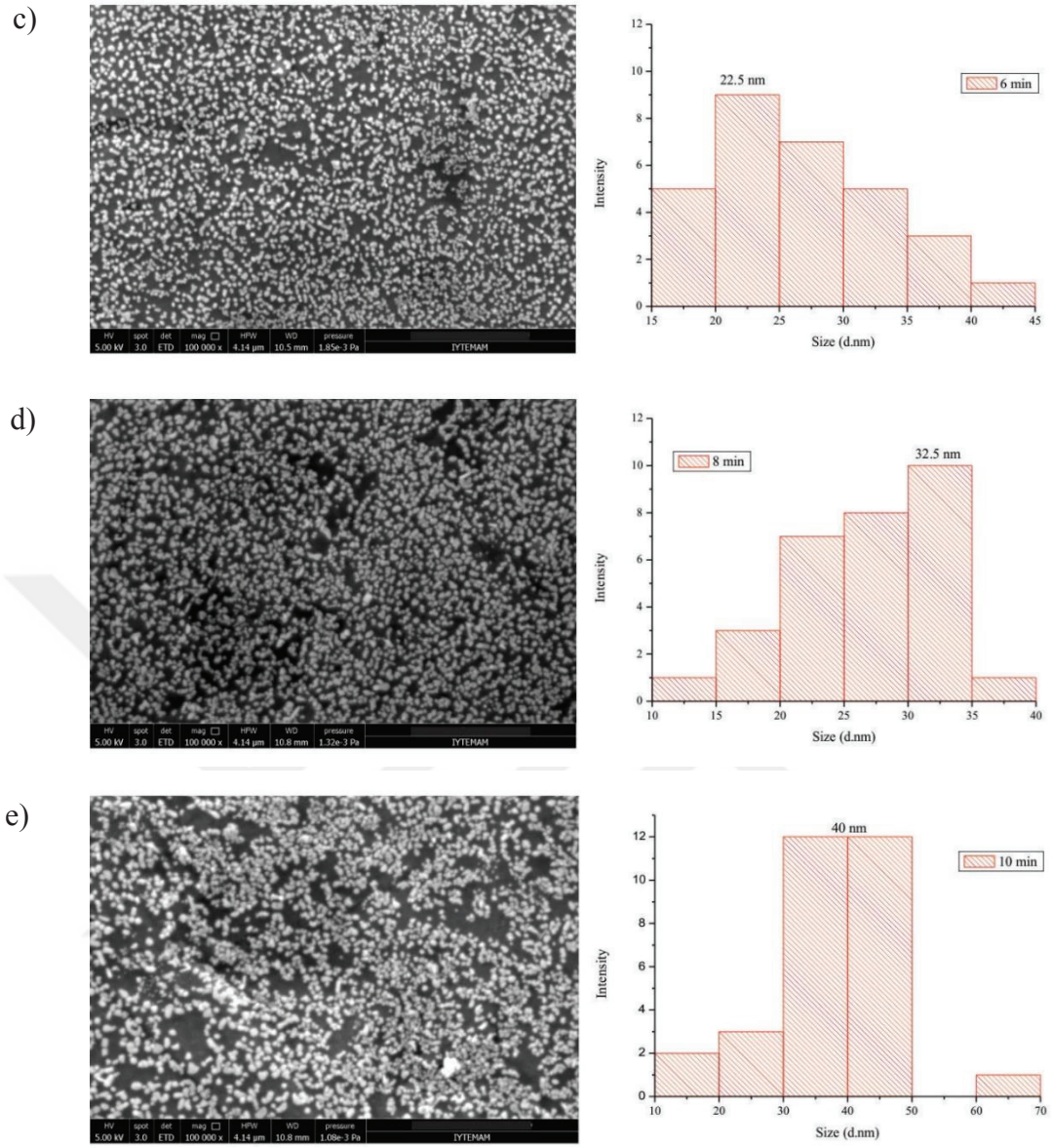

Figure 4.27. (cont)

Surface coverage ratio after gold growth was also calculated through the analysis of SEM images with ImageJ software. The percent surface coverage on solid support increased during growth as given in Fig. 4.28. The increased surface coverage; from 15% to 85% in 10 mins growing time, is the indication of gold growing on solid support. Table 4. 2 summarize the average percent of surface coverage of GNPs depending on gold growing time.

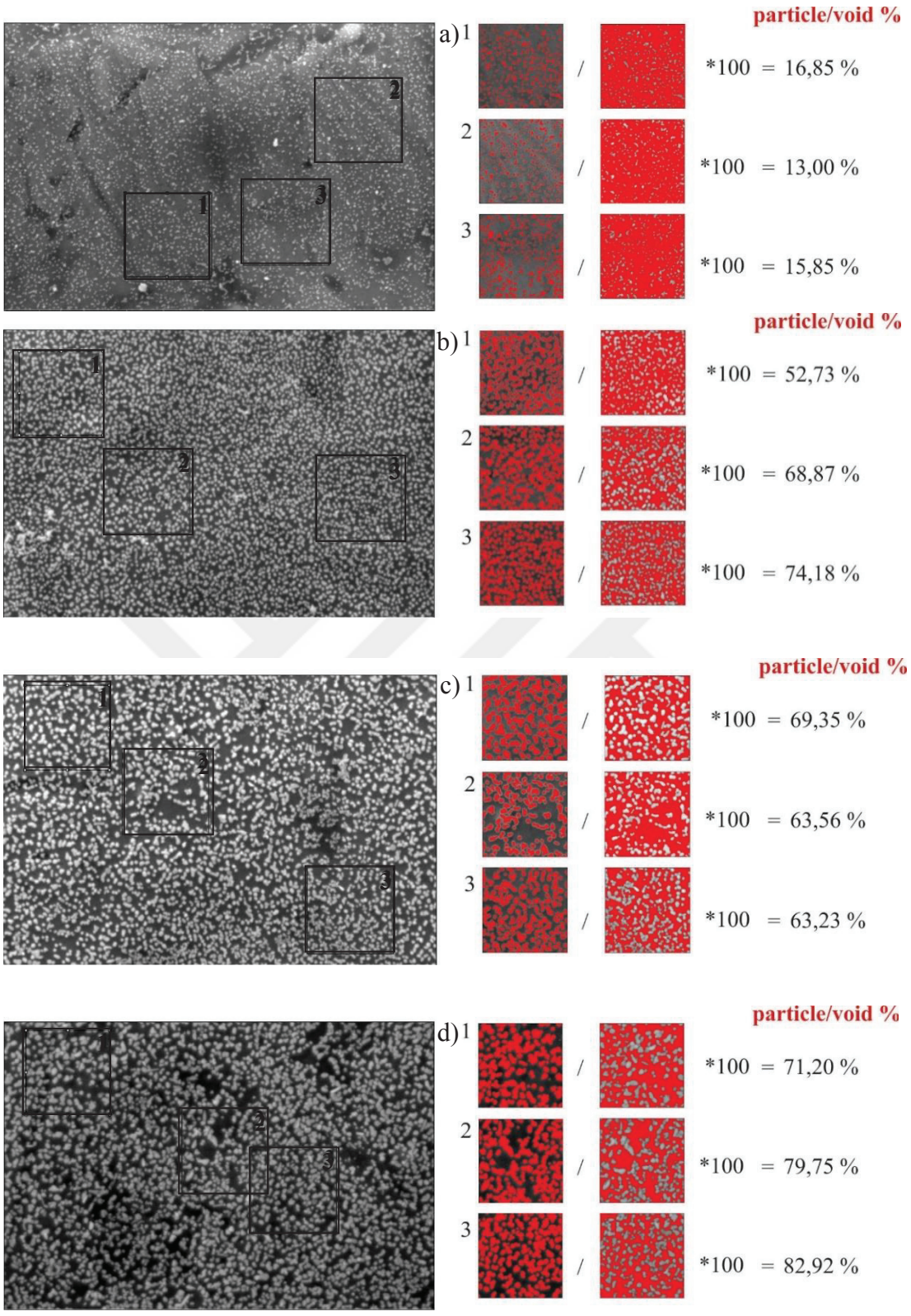

Figure 4.28. Surface coverage and percent particle analysis against void obtained from SEM images for a) the immobilized GNPs (0 min) b-e) the gold growth on solid support at 4, 6, 8 and 10 min.

(cont. on next page)

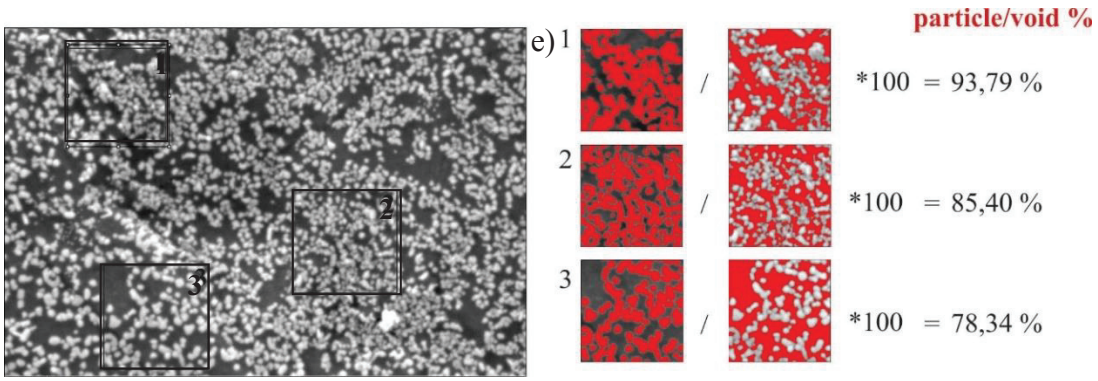

Figure 4.28. (cont.)

Table 4.2. Average of GNP percent surface coverage on the solid surface depending on gold growing time

Growth time (min)	Average particle%
0	15,23
4	65,26
6	65,38
8	82,92
10	85,84

4.3.2.2. AFM Analysis

Figure 4.29 illustrates the AFM images obtained from GNP immobilized and gold growth surfaces. Surface topographies in the first column support uniform seeding and growth of GNPs on solid surface. The height profile of the corresponding area indicates while the average height of immobilized gold particles from the surface is 11 nm, the 1, 2 and 3 min gold growth surfaces' average vertical height varies from 13 nm to 15 nm respectively as shown in Figure 4.29 b-d. Moreover, the 3D images demonstrate that surface thickness varies around 20 to 25, 1 nm during 3 min gold growing.

The surface coverage is increasing with growing time which causes agglomeration and so electric charge is increasing by the mechanical stress. That's why, longer growing times were also analyzed but the AFM tip was not sensitive enough to differentiate the surfaces and AFM images could not be taken clearly for further growth GNPs.

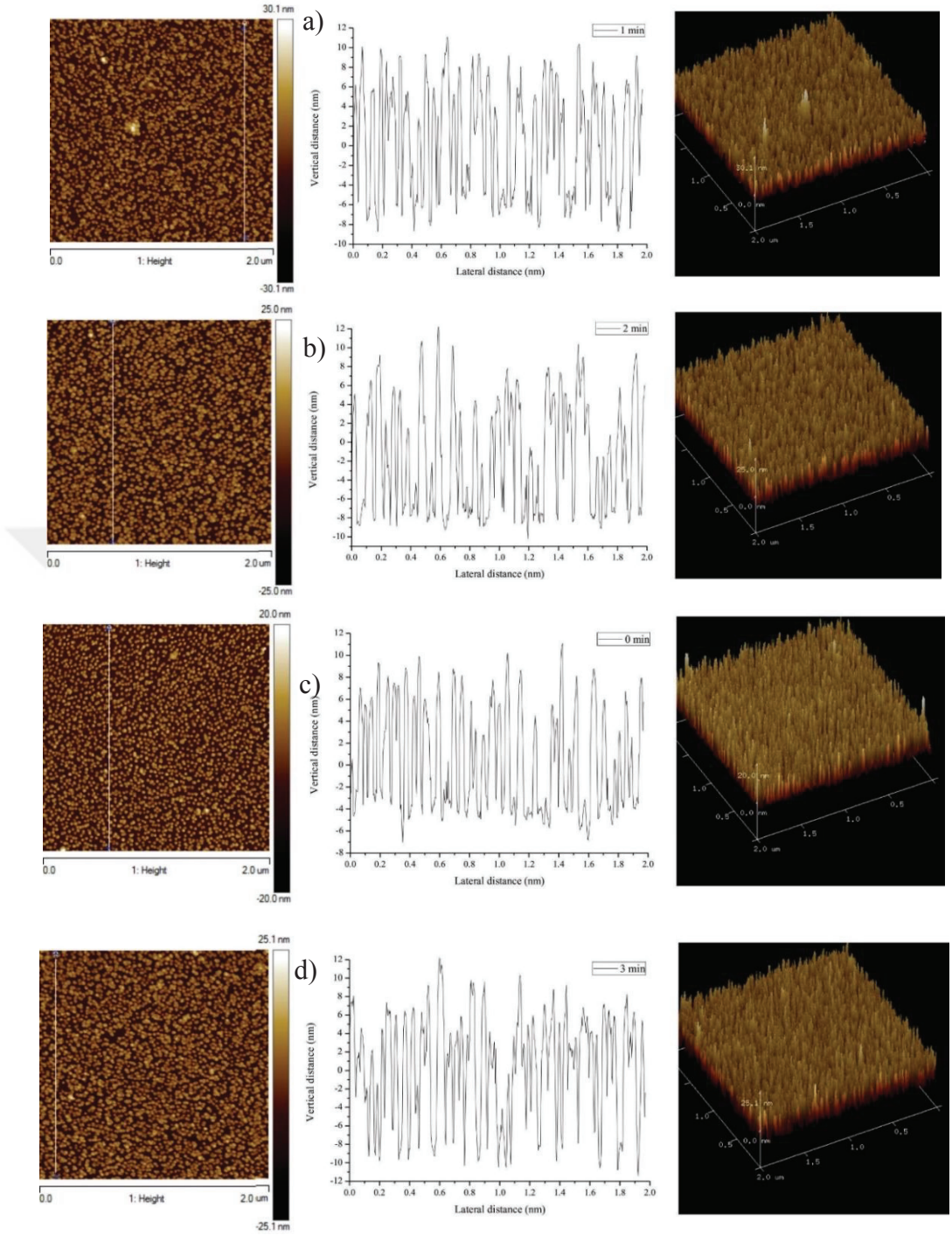

Figure 4.29. AFM images of a) immobilized GNPs (0 min) and b, c, d) gold growth surfaces on solid support at 1, 2 and 3 min respectively. The second column shows a cross-section profile along the white line shown in the first column The third column represents the corresponding 3D topography of the surfaces

4.4. Bacteria Detection

Two bacterial strains; BL21(DE3) and DH5 alpha were used for bacteria detection studies. Overnight growth media was used when it reached to stationary phase that is confirmed with continuous monitoring at 600 nm as shown in Figure 4.30.

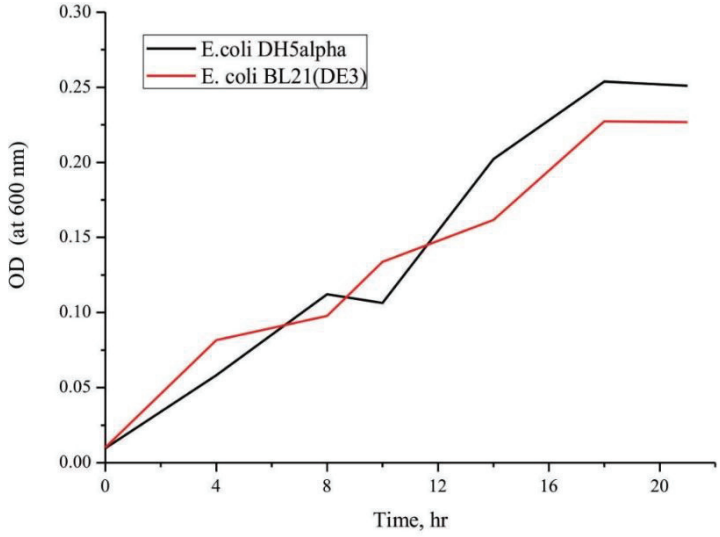

Figure 4.30. *E. coli* BL21(DE3) and *E. coli* DH5alpha bacteria growing curve at 600 nm

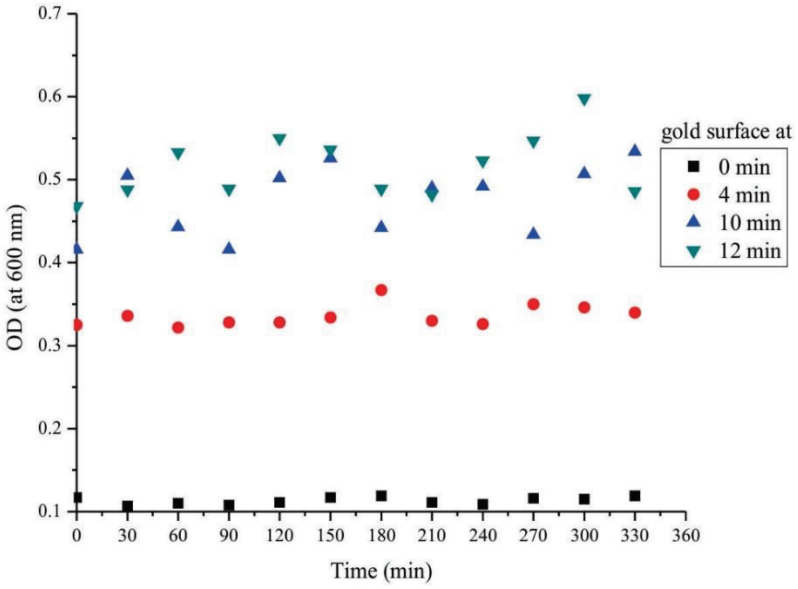

Figure 4.31. Time dependent bacteria BL21(DE3) adsorption on to the gold surfaces, monitored at 600 nm

To monitor the continuous growth and immobilization of bacteria directly on gold surface, the BL21(DE3) bacterial strain in LB Broth were loaded as 100 µL onto non-growth and 4, 10 and 12 min gold growing surfaces. Absorbance changes at 600nm were measured at every 30 min up to 330 min after rinsing three times with PBS (Fig 4.31). Fig 4.31 shows the adsorption behavior of bacteria directly on gold surface. Hence gold surface is negatively charged due to citrate capping it is expected that negatively charged gram-negative bacteria cannot attach directly onto gold surface as seen in non-growth surface (Fig 4.31). However, at 4, 10 and 12 min gold growth surfaces, bacteria are attached on to gold surface due to changing surface structure. Furthermore, adsorption behavior of bacteria was investigated on non-growth and gold growth surfaces as shown in Fig 4.32 that optimal binding time for bacteria screening through LSPR is around 90 mins which is confirmed by a spectral shift.

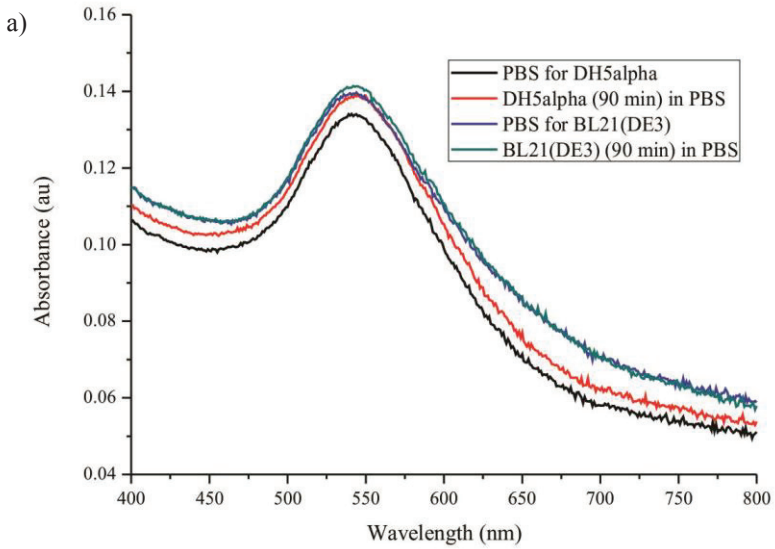

Figure 4.32. Comparison of *E. coli* BL21(DE3) and *E. coli* DH5alpha adsorption at 90 min on to a) the GNP immobilized surface (0 min) b) the gold growth surface (4 min)

(cont. on next page)

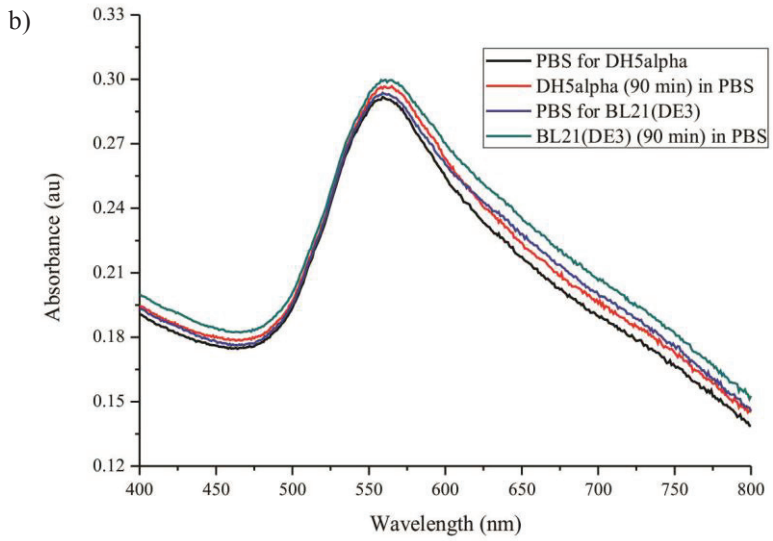

Figure 4.32. (cont.)

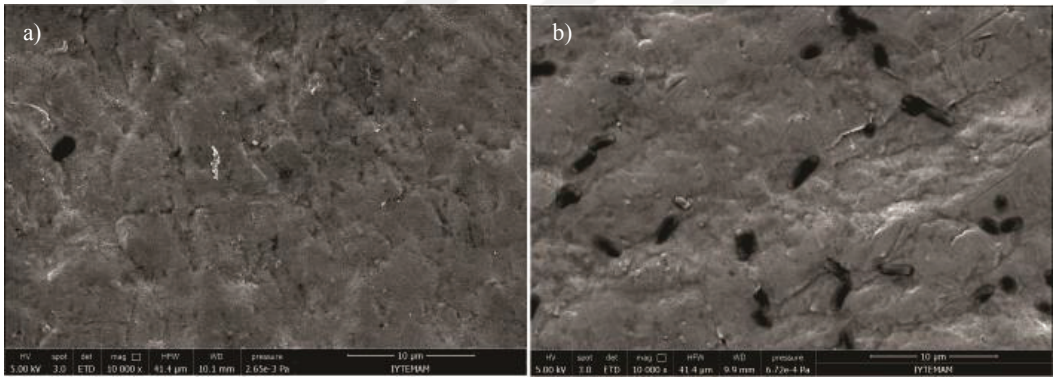

Figure 4.33. *E. coli* BL21(DE3) 30 min adsorption on a) the GNPs surface b) the PLL surface (scale bar: 10 µm)

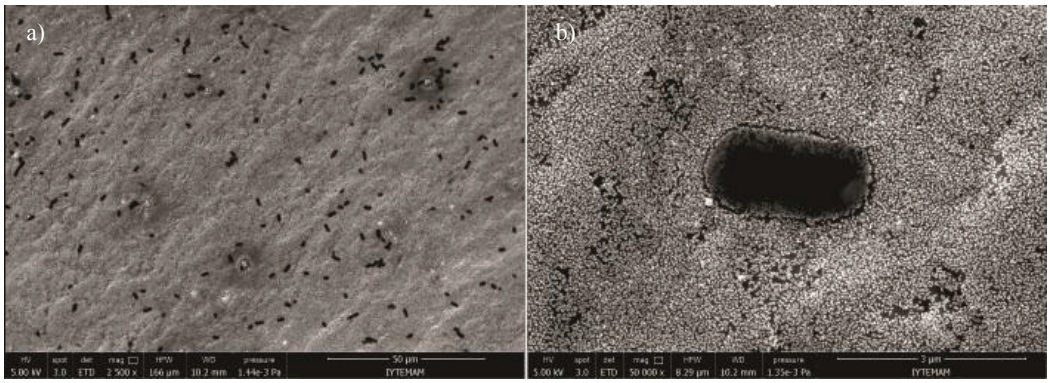

Figure 4.34. *E. coli* BL21(DE3) 30 min adsorption on the 4 min growth GNPs surface scale bar at a) 50 µm b) 3 µm

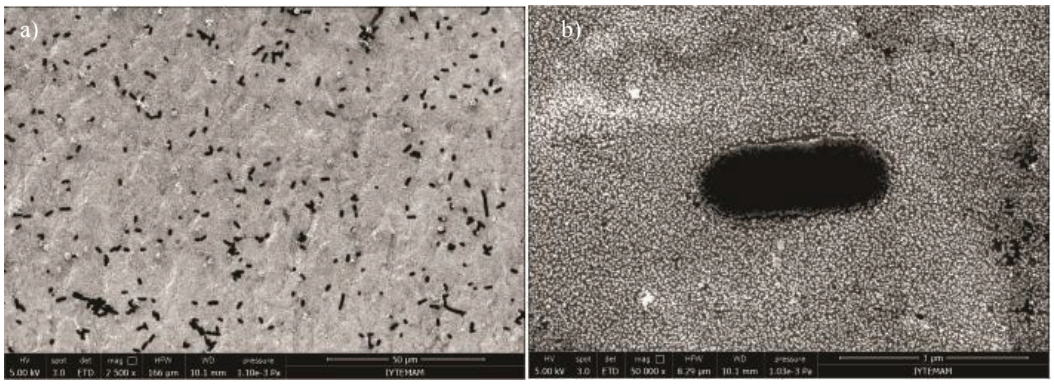

Figure 4.35. *E. coli* BL21(DE3) 30 min adsorption on the 10 min growth GNPs surface scale bar at a) 50 µm b) 3 µm

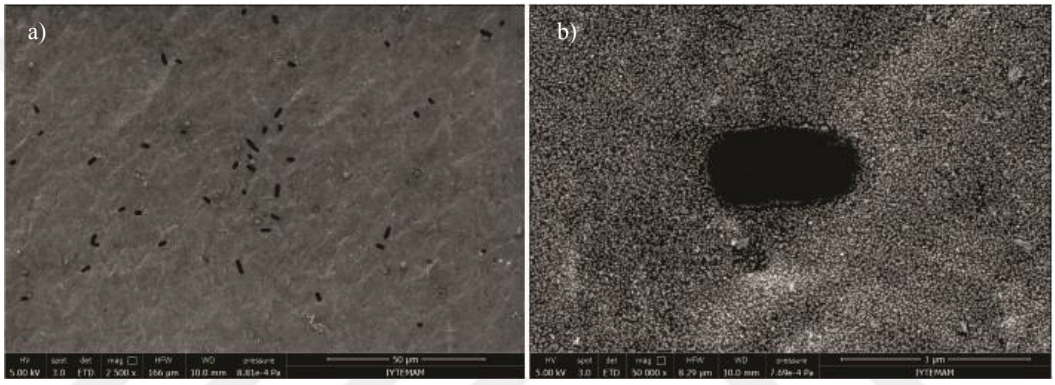

Figure 4.36. *E. coli* BL21(DE3) 60 min adsorption on the 4 min growth GNPs surface scale bar at a) 50 µm b) 3 µm

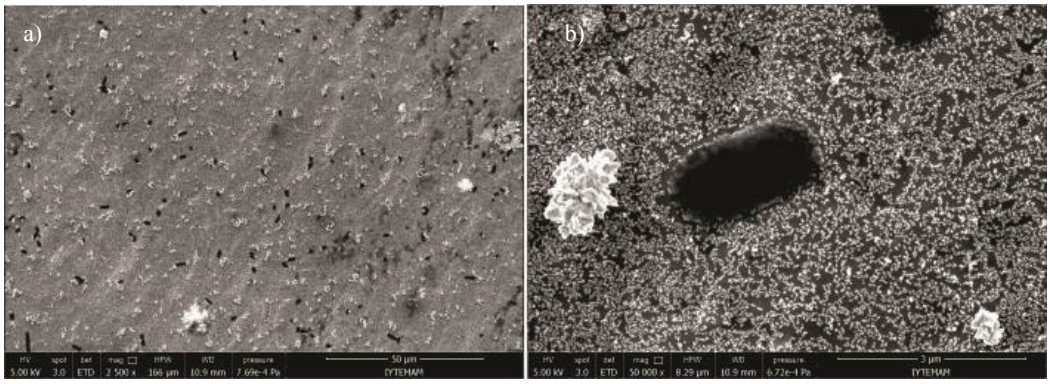

Figure 4.37. *E. coli* BL21(DE3) 60 min adsorption on the 10 min growth GNPs surface scale bar at a) 50 µm b) 3 µm

After overnight incubation of *E. coli* BL21(DE3) in LB Broth which had 0,106 OD value (about 8,5*10^7 bacteria concentration) at 600 nm. Figures from 4.33 to 4.37 show the bacteria adsorption on gold surface, which is increasing with gold growth. SEM images correlate with previous findings seen in Fig 4.31.

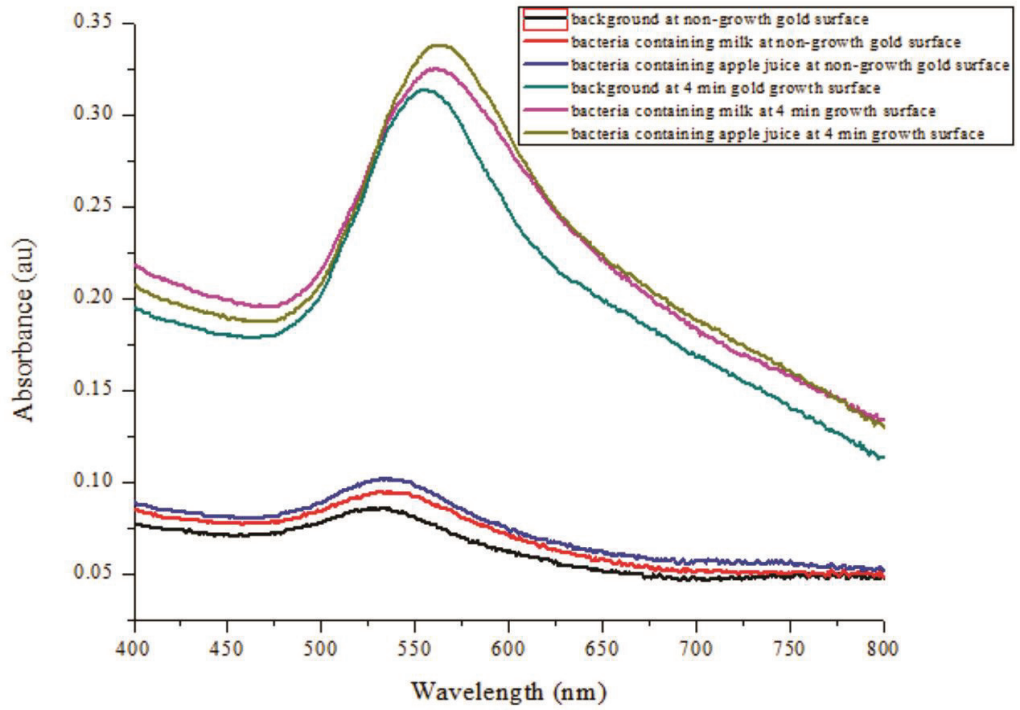

Figure 4.38. Absorbance spectrum of *E. coli* BL21(DE3) in milk and apple juice on the non-growth gold surfaces and the 4 min gold growth surfaces

To utilize the developed plasmonic platform as a biosensor commercial products were used for bacterial screening. Overnight growth *E. coli* BL21(DE3) culture is spiked into commercial milk and apple juice samples. The OD values was 0,094 in juice and 0,068 in milk at 600 nm which corresponds to about 7,5*10^7 and 5,4 *10^7 bacteria concentration respectively. The spectra were taken in water after 30 min incubation time. Fig. 4.38 represents that the red shift in plasmonic peak was increased with gold growth; while, there was an about 4 nm shift for bacteria into both milk and juice on non-growth gold surface, there was an about 6 nm shift for bacteria in milk and 8 nm shift for bacteria in juice on gold growth surface. This shows us increased sensitivity on growth surface which corresponds to capability of the developed plasmonic platform as a LSPR biosensor.

CHAPTER 5

CONCLUSION

The plasmonic solid platform that exhibit significant refractive index sensitivity was developed to detect the *E. coli* bacteria strains. The immobilized gold nanoparticle on the polystyrene solid substrates were subjected to grow by strong and mild reducing agents enabling to control shift in plasmonic wavelength. The gold growing on solid state gold surface was achieved with 20 µL $HAuCl_4$ and 80 µL NH_2OH. It was found that ascorbic acid is not effective reducing agent at gold seeded growth process in the proposed methodology. The size of the particles are controlled with duration time of the growth solution on the surface. The bacterial adsorption on the gold surfaces was made with *E. coli* DH5alpha and *E. coli* BL21(DE3) with around 10^7 cfu/ml. The binding kinetic of the bacteria to growth gold surface increased for the substrate that subjected to longer growing period. The ANN results showed that analyzing the all spectrum data can provide a better estimation of unknown sample concentration than LSPR peak shift. As a conclusion, the proposed LSPR-based label free methodology is promising to be an alternative to the bacteria screening in water or food samples. Moreover, the application of this methodology can be used in various field; bacteria strain differentiation without using general techniques like ELISA has been shown in this study as just one example. This study provides label free, simple and cost-effective strategy to enhance refractive index sensitivity and enables use in many biosensensing applications.

REFERENCES

1. Nagarajan, R., Nanoparticles: building blocks for nanotechnology. ACS Publications: 2008.

2. Shi, W.; Sahoo, Y.; Swihart, M. T.; Prasad, P., Gold nanoshells on polystyrene cores for control of surface plasmon resonance. *Langmuir* **2005,** *21* (4), 1610-1617.

3. Poon, C.-Y.; Chan, H.-M.; Li, H.-W., Direct detection of prostate specific antigen by darkfield microscopy using single immunotargeting silver nanoparticle. *Sensors and Actuators B: Chemical* **2014,** *190*, 737-744.

4. Gong, T.; Olivo, M.; Dinish, U.; Goh, D.; Kong, K. V.; Yong, K.-T., Engineering bioconjugated gold nanospheres and gold nanorods as label-free plasmon scattering probes for ultrasensitive multiplex dark-field imaging of cancer cells. *Journal of biomedical nanotechnology* **2013,** *9* (6), 985-991.

5. Eustis, S.; El-Sayed, M. A., Why gold nanoparticles are more precious than pretty gold: noble metal surface plasmon resonance and its enhancement of the radiative and nonradiative properties of nanocrystals of different shapes. *Chemical society reviews* **2006,** *35* (3), 209-217.

6. Katherine A. Willets, W. P. H., Leif J. Sherry, Xiaoyu Zhang, Jing Zhao, and Richard P. Van Duyne, Nanoscale Localized Surface Plasmon Resonance Biosensors. Nanobiotechnology II, 2007; pp 159-173.

7. Willets, K. A.; Van Duyne, R. P., Localized surface plasmon resonance spectroscopy and sensing. *Annu Rev Phys Chem* **2007,** *58*, 267-97.

8. Martinsson, E.; Sepulveda, B.; Chen, P.; Elfwing, A.; Liedberg, B.; Aili, D., Optimizing the refractive index sensitivity of plasmonically coupled gold nanoparticles. *Plasmonics* **2014,** *9* (4), 773-780.

9. Jain, P. K.; El-Sayed, M. A., Noble metal nanoparticle pairs: effect of medium for enhanced nanosensing. *Nano letters* **2008,** *8* (12), 4347-4352.

10. Su, K.-H.; Wei, Q.-H.; Zhang, X.; Mock, J.; Smith, D. R.; Schultz, S., Interparticle coupling effects on plasmon resonances of nanogold particles. *Nano letters* **2003,** *3* (8), 1087-1090.

11. Weinrib, H.; Meiri, A.; Duadi, H.; Fixler, D., Uniformly Immobilizing Gold Nanorods on a Glass Substrate. *Journal of Atomic, Molecular, and Optical Physics* **2012,** *2012*, 1-6.

12. Shamaila, S.; Zafar, N.; Riaz, S.; Sharif, R.; Nazir, J.; Naseem, S., Gold Nanoparticles: An Efficient Antimicrobial Agent against Enteric Bacterial Human Pathogen. *Nanomaterials (Basel)* **2016,** *6* (4).

13. Leng, W.; Pati, P.; Vikesland, P. J., Room temperature seed mediated growth of gold nanoparticles: mechanistic investigations and life cycle assesment. *Environ. Sci.: Nano* **2015,** *2* (5), 440-453.

14. Yuan, L.; Wang, X.; Fang, Y.; Liu, C.; Jiang, D.; Wo, X.; Wang, W.; Chen, H. Y., Digitizing Gold Nanoparticle-Based Colorimetric Assay by Imaging and Counting Single Nanoparticles. *Anal Chem* **2016,** *88* (4), 2321-6.

15. Jain, P. K.; Huang, W.; El-Sayed, M. A., On the universal scaling behavior of the distance decay of plasmon coupling in metal nanoparticle pairs: a plasmon ruler equation. *Nano Letters* **2007,** *7* (7), 2080-2088.

16. Boisselier, E.; Astruc, D., Gold nanoparticles in nanomedicine: preparations, imaging, diagnostics, therapies and toxicity. *Chem Soc Rev* **2009,** *38* (6), 1759-82.

17. Pong, B.-K.; Elim, H. I.; Chong, J.-X.; Ji, W.; Trout, B. L.; Lee, J.-Y., New insights on the nanoparticle growth mechanism in the citrate reduction of gold (III) salt: formation of the Au nanowire intermediate and its nonlinear optical properties. *The Journal of Physical Chemistry C* **2007,** *111* (17), 6281-6287.

18. Toshima, N.; Yonezawa, T., Bimetallic nanoparticles—novel materials for chemical and physical applications. *New Journal of Chemistry* **1998,** *22* (11), 1179-1201.

19. Jana, N. R.; Gearheart, L.; Murphy, C. J., Wet chemical synthesis of high aspect ratio cylindrical gold nanorods. *The Journal of Physical Chemistry B* **2001,** *105* (19), 4065-4067.

20. Fattori, N.; Maroneze, C. M.; Da Costa, L. P.; Strauss, M.; Mazali, I. O.; Gushikem, Y., Chemical and photochemical formation of gold nanoparticles supported on viologen-functionalized SBA-15. *Colloids and Surfaces A: Physicochemical and Engineering Aspects* **2013,** *437*, 120-126.

21. Zhang, J.; Du, J.; Han, B.; Liu, Z.; Jiang, T.; Zhang, Z., Sonochemical formation of single- crystalline gold nanobelts. *Angewandte Chemie* **2006,** *118* (7), 1134-1137.

22. Okitsu, K.; Ashokkumar, M.; Grieser, F., Sonochemical synthesis of gold nanoparticles: effects of ultrasound frequency. *The Journal of Physical Chemistry B* **2005,** *109* (44), 20673-20675.

23. Raj, M. A.; John, S. A., Fast growth of gold nanorods on solid substrate using electrochemically deposited gold seeds. *Electrochemistry Communications* **2014,** *45*, 27-31.

24. Akhavan, A.; Kalhor, H.; Kassaee, M.; Sheikh, N.; Hassanlou, M., Radiation synthesis and characterization of protein stabilized gold nanoparticles. *Chemical Engineering Journal* **2010,** *159* (1), 230-235.

25. Wender, H.; Andreazza, M. L.; Correia, R. R.; Teixeira, S. R.; Dupont, J., Synthesis of gold nanoparticles by laser ablation of an Au foil inside and outside ionic liquids. *Nanoscale* **2011,** *3* (3), 1240-1245.

26. Amendola, V.; Meneghetti, M., Laser ablation synthesis in solution and size manipulation of noble metal nanoparticles. *Physical chemistry chemical physics* **2009,** *11* (20), 3805-3821.

27. Iqbal, M.; Usanase, G.; Oulmi, K.; Aberkane, F.; Bendaikha, T.; Fessi, H.; Zine, N.; Agusti, G.; Errachid, E.-S.; Elaissari, A., Preparation of gold nanoparticles and determination of their particles size via different methods. *Materials Research Bulletin* **2016,** *79*, 97-104.

28. Brown, K. R.; Walter, D. G.; Natan, M. J., Seeding of colloidal Au nanoparticle solutions. 2. Improved control of particle size and shape. *Chemistry of Materials* **2000,** *12* (2), 306-313.

29. Zhao, P.; Li, N.; Astruc, D., State of the art in gold nanoparticle synthesis. *Coordination Chemistry Reviews* **2013,** *257* (3-4), 638-665.

30. Turkevich, J.; Stevenson, P. C.; Hillier, J., A study of the nucleation and growth processes in the synthesis of colloidal gold. *Discussions of the Faraday Society* **1951,** *11*, 55-75.

31. Faraday, M., The Bakerian lecture: experimental relations of gold (and other metals) to light. *Philosophical Transactions of the Royal Society of London* **1857,** *147*, 145-181.

32. Frens, G., Controlled nucleation for the regulation of the particle size in monodisperse gold suspensions. *Nature* **1973,** *241* (105), 20-22.

33. Kumar, S.; Gandhi, K.; Kumar, R., Modeling of formation of gold nanoparticles by citrate method. *Industrial & Engineering Chemistry Research* **2007,** *46* (10), 3128-3136.

34. Slot, J. W.; Geuze, H. J., A new method of preparing gold probes for multiple-labeling cytochemistry. *European journal of cell biology* **1985,** *38* (1), 87-93.

35. Brown, K. R.; Fox, A. P.; Natan, M. J., Morphology-dependent electrochemistry of cytochrome c at Au colloid-modified SnO2 electrodes. *Journal of the American Chemical Society* **1996,** *118* (5), 1154-1157.

36. Brust, M.; Walker, M.; Bethell, D.; Schiffrin, D. J.; Whyman, R., Synthesis of thiol-derivatised gold nanoparticles in a two-phase liquid–liquid system. *Journal of the Chemical Society, Chemical Communications* **1994,** (7), 801-802.

37. Schmid, G.; Pfeil, R.; Boese, R.; Bandermann, F.; Meyer, S.; Calis, G.; van der Velden, J. W., Au55 [P (C6H5) 3] 12CI6—ein Goldcluster ungewöhnlicher Größe. *European Journal of Inorganic Chemistry* **1981,** *114* (11), 3634-3642.

38. Weare, W. W.; Reed, S. M.; Warner, M. G.; Hutchison, J. E., Improved synthesis of small (d core≈ 1.5 nm) phosphine-stabilized gold nanoparticles. *Journal of the American Chemical Society* **2000,** *122* (51), 12890-12891.

39. Moores, A.; Goettmann, F.; Sanchez, C.; Le Floch, P., Phosphinine stabilised gold nanoparticles; synthesis and immobilisation on mesoporous materials. *Chemical Communications* **2004,** (24), 2842-2843.

40. Shem, P. M.; Sardar, R.; Shumaker-Parry, J. S., One-step synthesis of phosphine-stabilized gold nanoparticles using the mild reducing agent 9-BBN. *Langmuir* **2009,** *25* (23), 13279-13283.

41. Seoudi, R.; Said, D. A., Studies on the effect of the capping materials on the spherical gold nanoparticles catalytic activity. *World Journal of Nano Science and Engineering* **2011,** *1* (02), 51.

42. Huang, H.; Yang, X., Synthesis of chitosan-stabilized gold nanoparticles in the absence/presence of tripolyphosphate. *Biomacromolecules* **2004,** *5* (6), 2340-2346.

43. Beveridge, T.; Murray, R., Sites of metal deposition in the cell wall of Bacillus subtilis. *Journal of bacteriology* **1980,** *141* (2), 876-887.

44. Jana, N. R.; Gearheart, L.; Murphy, C. J., Evidence for seed-mediated nucleation in the chemical reduction of gold salts to gold nanoparticles. *Chemistry of Materials* **2001,** *13* (7), 2313-2322.

45. Brown, K. R.; Lyon, L. A.; Fox, A. P.; Reiss, B. D.; Natan, M. J., Hydroxylamine seeding of colloidal Au nanoparticles. 3. Controlled formation of conductive Au films. *Chemistry of Materials* **2000,** *12* (2), 314-323.

46. Jana, N. R.; Gearheart, L.; Murphy, C. J., Seed-mediated growth approach for shape-controlled synthesis of spheroidal and rod-like gold nanoparticles using a surfactant template. *Advanced Materials* **2001,** *13* (18), 1389.

47. Nikoobakht, B.; El-Sayed, M. A., Preparation and growth mechanism of gold nanorods (NRs) using seed-mediated growth method. *Chem. Mater* **2003,** *15* (10), 1957-1962.

48. Cataldi, U.; Caputo, R.; Kurylyak, Y.; Klein, G.; Chekini, M.; Umeton, C.; Bürgi, T., Growing gold nanoparticles on a flexible substrate to enable simple mechanical control of their plasmonic coupling. *Journal of Materials Chemistry C* **2014,** *2* (37), 7927.

49. Brown, K. R.; Natan, M. J., Hydroxylamine seeding of colloidal Au nanoparticles in solution and on surfaces. *Langmuir* **1998,** *14* (4), 726-728.

50. Zhao, J.; Zhang, X.; Yonzon, C. R.; Haes, A. J.; Van Duyne, R. P., Localized surface plasmon resonance biosensors. *Nanomedicine* **2006,** *1* (2), 219-228.

51. Stockman, M. I., Nanoplasmonic sensing and detection. *Science* **2015,** *348* (6232), 287-288.

52. Guo, L.; Jackman, J. A.; Yang, H.-H.; Chen, P.; Cho, N.-J.; Kim, D.-H., Strategies for enhancing the sensitivity of plasmonic nanosensors. *Nano Today* **2015,** *10* (2), 213-239.
53. Anker, J. N.; Hall, W. P.; Lyandres, O.; Shah, N. C.; Zhao, J.; Van Duyne, R. P., Biosensing with plasmonic nanosensors. *Nature materials* **2008,** *7* (6), 442-453.

54. Huang, K. C.; Mukhopadhyay, R.; Wen, B.; Gitai, Z.; Wingreen, N. S., Cell shape and cell-wall organization in Gram-negative bacteria. *Proc Natl Acad Sci U S A* **2008,** *105* (49), 19282-7.

55. Brzozowska, E.; Koba, M.; Śmietana, M.; Górska, S.; Janik, M.; Gamian, A.; Bock, W. J., Label-free Gram-negative bacteria detection using bacteriophage-adhesin-coated long-period gratings. *Biomedical optics express* **2016,** *7* (3), 829-840.

56. Verma, M. S.; Rogowski, J. L.; Jones, L.; Gu, F. X., Colorimetric biosensing of pathogens using gold nanoparticles. *Biotechnology advances* **2015,** *33* (6), 666-680.

57. Wang, Y.; Alocilja, E. C., Gold nanoparticle-labeled biosensor for rapid and sensitive detection of bacterial pathogens. *Journal of biological engineering* **2015,** *9* (1), 16.

58. Oh, B.-K.; Lee, W.; Kim, Y.-K.; Lee, W. H.; Choi, J.-W., Surface plasmon resonance immunosensor using self-assembled protein G for the detection of Salmonella paratyphi. *Journal of biotechnology* **2004,** *111* (1), 1-8.

59. Li, Y.; Yan, X.; Feng, X.; Wang, J.; Du, W.; Wang, Y.; Chen, P.; Xiong, L.; Liu, B.-F., Agarose-based microfluidic device for point-of-care concentration and detection of pathogen. *Analytical chemistry* **2014,** *86* (21), 10653-10659.

60. Sun, J.; Ge, J.; Liu, W.; Wang, X.; Fan, Z.; Zhao, W.; Zhang, H.; Wang, P.; Lee, S.-T., A facile assay for direct colorimetric visualization of lipopolysaccharides at low nanomolar level. *Nano Research* **2012,** *5* (7), 486-493.

61. Li, X. X.; Cao, C.; Han, S. J.; Sim, S. J., Detection of pathogen based on the catalytic growth of gold nanocrystals. *water research* **2009,** *43* (5), 1425-1431.

62. Zetasizer nano series user manual_Man0317-1.1. **2004**.

63. ATA Scientific. Dynamic Light Scattering Training. Malvern Zetasizer LS.

64. GE Healthcare Life Sciences. Spectrophotometry. Handbook.

65. Behera, S.; Ghanty, S.; Ahmad, F.; Santra, S.; Banerjee, S., UV-visible spectrophotometric method development and validation of assay of paracetamol tablet formulation. *J Anal Bioanal Techniques* **2012,** *3* (6), 151-157.

66. Vernon-Parry, K. D.; Scanning Electron Microscopy: an introduction. *Analysis* **2000,** 13 (4)

67. Bogner, A.; Jouneau, P. H.; Thollet, G.; Basset, D.; Gauthier, C., A history of scanning electron microscopy developments: towards "wet-STEM" imaging. *Micron* **2007,** *38* (4), 390-401.

68. PI Technology. Electron Microscopy: Nonmagnetic Drives and Stages for Vacuum. www.pi-usa.us/blog/electron-microscopy-nonmagnonmagnetic-vacuum-compatible-and-high-precision-drives-and-positioning-systems-for-electron-microscopesnetic-drives-stages-for-vacuum/ (accessed May 24, 2017).

69. Jalili, N.; Laxminarayana, K., A review of atomic force microscopy imaging systems: application to molecular metrology and biological sciences. *Mechatronics* **2004,** *14* (8), 907-945.

70. Yang, H.; Wang, Y.; Lai, S.; An, H.; Li, Y.; Chen, F., Application of atomic force microscopy as a nanotechnology tool in food science. *J Food Sci* **2007,** *72* (4), R65-75.

71. Binnig, G.; Quate, C. F.; Gerber, C., Atomic force microscope. *Phys Rev Lett* **1986,** *56* (9), 930-933.

72. Amato, F.; López, A.; Peña-Méndez, E. M.; Vaňhara, P.; Hampl, A.; Havel, J., Artificial neural networks in medical diagnosis. Elsevier: 2013.

73. Malik, B. A.; Naqash, A.; Bhat, G. M. In *Backpropagation artificial neural network for determination of glucose concentration from near-infrared spectra*, Advances in Computing, Communications and Informatics (ICACCI), 2016 International Conference on, IEEE: 2016; pp 2688-2691.

74. Mohamad-Saleh, J.; Hoyle, B. S., Improved neural network performance using principal component analysis on Matlab. *International journal of the computer, the internet and Management* **2008,** *16* (2), 1-8.

75. Ioele, G.; De Luca, M.; Dinç, E.; Oliverio, F.; Ragno, G., Artificial neural network combined with principal component analysis for resolution of complex pharmaceutical formulations. *Chemical and Pharmaceutical Bulletin* **2011,** *59* (1), 35-40.

76. Kumar, S.; Yang, H.; Zou, S., Seed-mediated growth of uniform gold nanoparticle arrays. *The Journal of Physical Chemistry C* **2007,** *111* (35), 12933-12938.

77. Evcimen, N. I.; Coskun, S.; Kozanoglu, D.; Ertas, G.; Unalan, H. E.; Nalbant Esenturk, E., Growth of branched gold nanoparticles on solid surfaces and their use as surface-enhanced Raman scattering substrates. *RSC Adv.* **2015,** *5* (123), 101656-101663.

78. Tabakman, S. M.; Chen, Z.; Casalongue, H. S.; Wang, H.; Dai, H., A new approach to solution-phase gold seeding for SERS substrates. *Small* **2011,** *7* (4), 499-505.

79. Cytodiagnostics. Introduction to Gold Nanoparticle Characterization. http://www.cytodiagnostics.com/store/pc/Introduction-to-Gold-Nanoparticle-Characterization-d3.htm (accessed May 30, 2017).